AFAPL-TR-71-45

RESEARCH ON NONEQUILIBRIUM MHD GENERATORS

J. L. Kerrebrock
Massachusetts Institute of Technology

TECHNICAL REPORT, AFAPL-TR-71-45

July 1971

Air Force Aero Propulsion Laboratory
Air Force Systems Command
Wright-Patterson Air Force Base, Ohio

NOTICE

When Government drawings, specifications, or other data are used for any purpose other than in connection with a definitely related Government procurement operation, the United States Government thereby incurs no responsibility nor any obligation whatsoever; and the fact that the government may have formulated, furnished, or in any way supplied the said drawings, specifications, or other data, is not to be regarded by implication or otherwise as in any manner licensing the holder or any other person or corporation, or conveying any rights or permission to manufacture, use, or sell any patented invention that may in any way be related thereto.

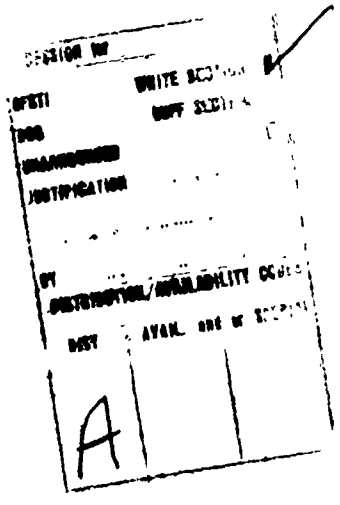

Copies of this report should not be returned unless return is required by security considerations, contractual obligations, or notice on a specific document.

UNCLASSIFIED

Security Classification

DOCUMENT CONTROL DATA - R & D

(Security classification of title, body of abstract and indexing annotation must be entered when the overall report is classified)

1 ORIGINATING ACTIVITY *(Corporate author)*

Massachusetts Institute of Technology
Space Propulsion Laboratory
Cambridge, Massachusetts 02139

2a. REPORT SECURITY CLASSIFICATION

Unclassified

2b GROUP

None

3 REPORT TITLE

RESEARCH ON NONEQUILIBRIUM MHD GENERATORS

4 DESCRIPTIVE NOTES *(Type of report and inclusive dates)*

Annual Technical Progress Report. Work conducted during February 1970 and December 1970

5 AUTHOR(S) *(First name, middle initial, last name)*

Kerrebrock, J. L.

6 REPORT DATE	7a. TOTAL NO OF PAGES	7b. NO OF REFS
July 1971	43	

8a CONTRACT OR GRANT NO	9a. ORIGINATOR'S REPORT NUMBER(S)
F33615-69-C-1226	
b PROJECT NO: 3145	
c	9b. OTHER REPORT NO(S) *(Any other numbers that may be assigned this report)*
d	AFAPL-TR-71-45

10 DISTRIBUTION STATEMENT

Distribution of this document is unlimited.

11 SUPPLEMENTARY NOTES	12 SPONSORING MILITARY ACTIVITY
	USAF Aero Propulsion Laboratory, POP-2 Air Force Systems Command Wright-Patterson Air Force Base, Ohio

13 ABSTRACT

A summary is presented of progress in a study of nonequilibrium generators, with emphasis on the vibrational excitation of molecular species. Experimental work on a large generator includes development of a coaxial preionizer and development of slanted electrode walls, both of which increase the power density of the generator. A three-dimensional analysis of the slanted electrode wall is also given. Finally a preliminary report is given of experimental and theoretical work on the effect of an intense radiation field, coupled to the molecules, on electrothermal instabilities.

DD FORM 1 NOV 1473

UNCLASSIFIED

Security Classification

14 KEY WORDS	LINK A		LINK B		LINK C	
	ROLE	WT	ROLE	WT	ROLE	WT
1. MHD Power Generation						
2. Nonequilibrium Plasmas						
3. Vibrational Excitation						
4. Ionization Instabilities						
5. Electrothermal Instabilities						
6. Lasers						

RESEARCH ON NONEQUILIBRIUM MHD GENERATORS

J. L. Kerrebrock
Massachusetts Institute of Technology

Air Force Aero Propulsion Laboratory
Air Force Systems Command
Wright-Patterson Air Force Base, Ohio

FOREWORD

This report was prepared by the Space Propulsion Laboratory of the Massachusetts Institute of Technology and covers work conducted from February 1, 1970 to December 31, 1970. It was submitted by the authors on

The work is being administered under the direction of the Air Force Aero Propulsion Laboratory, Directorate of Laboratories, Air Force Systems Command, United States Air Force. The USAF Project Engineer is Dr. James F. Holt (AFAPL/POP-2) with Robert F. Cooper (AFAPL/POP-2) the Technical Area Manager.

Space Propulsion Laboratory personnel participating in this research include:

Jack L. Kerrebrock	Professor, Aeronautics and Astronautics
Albert Solbes	Associate Professor, Aeronautics and Astronautics
Jean F. Louis	Associate Professor, Aeronautics and Astronautics
David A. Oliver	Assistant Professor, Aeronautics and Astronautics
Klaus Witte	Research Associate (Visiting from the Institute for Plasmaphysik, Garching)
Michael Hsu	Graduate Research Assistant, Aeronautics and Astronautics
Andrew Lowenstein	Graduate Research Assistant, Aeronautics and Astronautics

The work by this report was accomplished under United States Air Force Contract F33615-69-C-1226 Project No. 3145.

This technical report has been reviewed and is approved.

Richard G. Leiby

RICHARD G. LEIBY
Major, USAF
Chief, Laser and Aircraft Power Branch
Aerospace Power Division

ABSTRACT

A summary is presented of progress in a study of nonequilibrium generators, with emphasis on the vibrational excitation of molecular species. Experimental work on a large generator includes development of a coaxial preionizer and development of slanted electrode walls, both of which increase the power density of the generator. A three-dimensional analysis of the slanted electrode wall is also given. Finally a preliminary report is given of experimental and theoretical work on the effect of an intense radiation field, coupled to the molecules, on electrothermal instabilities.

TABLE OF CONTENTS

FIGURE	LIST OF ILLUSTRATIONS	PAGE

FIGURE	LIST OF ILLUSTRATIONS (Cont'd)	PAGE
III: 13	Poi, $\tilde{j}_n$, and Joule dissipation, distributions	35
III: 14	Current vectors on slantwall	36
III: 15	Current vector pattern in y-z cross section	37
III: 16	$\tilde{j}_n$, $\tilde{D}$, distributions on slantwall	38
III: 17	Current vectors on slantwall	39
III: 18	Current vector pattern in y-z cross section	40
III: 19	$\tilde{j}_n$, $\tilde{D}$ distributions on slantwall. Apex analysis	41
III: 20	Current pattern in symmetry plane	42
III: 21	Current distribution on electrode	43

I. INTRODUCTION

This report summarizes progress in a continuing study of advanced concepts in energy conversion. The general objectives of the program are to identify promising new methods of energy conversion, and to carry out the research required to determine their feasibility.

The work has, for this reporting period, concentrated on studies of nonequilibrium MHD generators, and in particular on two aspects, the behavior of slanted electrode walls, and the behavior of molecular species in the generator.

As noted in Annual Report No. 1 (1),the slanted wall promises to greatly alleviate the problems of electrode wall shorting, and the consequent limits on Hall field recovery. Some encouraging preliminary experimental results were given in Quarterly Technical Progress Report No. 22 (2). A preliminary finite-element analysis of the slant wall was also given at that time.

Shortly after this data was obtained the Inert Gas Heater suffered a mechanical failure, and has been inoperable. Repairs were begun in October 1970, and it will be in operation in January 1971. Meanwhile analysis of the data, and more detailed theoretical studies of the slant wall have proceeded, and will be reported here.

In a parallel program, the feasibility of vibrationally exciting molecular species in nonequilibrium MHD generators was demonstrated (3). Because of the Air Force's interest in such possibilities, the generator program was reoriented in September 1970 to place emphasis on the excitation of molecular species in nonequilibrium generators. Three problems were identified for study, namely 1) the design of electrode walls suitable for operation at the desired high Hall parameter and Mach number, 2) inlet relaxation and preionization under the same conditions, 3) the effect on electrothermal instabilities of strong coupling, through molecules, to an intense radiation flux.

The first two items are essentially continuations of past work, except that emphasis is put on maximizing internal dissipation, rather than on producing power. The last is new, and has motivated the design and construction of a small scale experiment, which will be described. Item three is also being studied theoretically, by numerical methods.

II. SUMMARY OF PROGRESS

2.1 Nonequilibrium Generator Experiment

As was noted, the Inert Gas Heater has been inoperable since May 1970. Our effort during this time has been given to study of the results obtained prior to that time, to conducting a cold flow test on the channel, and to development of a computer program for calculation of the flow through the channel. The following results have emerged.

Preionizer behavior:

The preionizer comprises a cathode near the throat of the axially segmented supersonic nozzle, and an anode near the channel entrance. A "spinning coil" is arranged to impress an axial magnetic field on the nozzle. It was observed that, with this spinning coil in operation, the channel produced near-ideal open circuit voltage, but when loaded it performed very poorly. Movies taken from the channel exit showed that this was due to a stratification of the plasma, in the UXB direction, produced by the preionizer current flowing along magnetic field lines from the cathode tip to the insulator walls. A frame of this movie, shown in Fig. (1a) exhibits this pattern. Fig. (1b) shows the same view with the spinning coil off. It exhibits a more uniform plasma, because in this operating mode the discharge was from the cathode tip to the nozzle throat. We conclude that the stratification reduced the effect conductivity in the channel, preventing large load currents. The preionizer has been modified by addition of anode ballast resistors to ensure a more uniform current distribution.

Gas dynamics:

There was some uncertainty in the gas dynamic behavior of the channel, with considerable evidence that shocks existed in the downstream section (2). Accordingly the channel side walls were replaced with plexiglass plates, and the complete assembly of preionizer, channel, and diffuser was tested in a supersonic wind tunnel loop. The channel is shown in place in Fig. (2.). A shadowgraph of the upstream portion of the channel, Fig. (3a), shows a weak oblique shock system originating from the preionizer nozzle. This was expected. Fig. (3b) shows two normal shocks in the downstream portion of the channel. Their locations agree with those inferred from wall pressure measurements. This offers an explanation of abrupt drops in open-circuit voltage reported in Ref. (1), as well as a cutoff of load current in the downstream half of the channel.

Electrode drops:

Comparison of the data from the flat wall and slant wall channels shows electrode drops of approximately 10 volts for the slant wall compared to approximately 40 volts for the flat wall. This improvement evidently results from current flow along the magnetic field lines.

2.2 Three Dimensional Analysis of Slanted Electrode Wall

The basic idea of the slanted electrode wall is to relieve the boundary condition imposed by the insulating segments of the electrode wall, by

allowing a flow of current to the wall, in the direction of the magnetic field. This is a three dimensional phenomenon, yet analyses of it have been essentially two-dimensional. A three dimensional analysis of the current and field structure is given in detail in section 3.1, for the case of constant conductivity. The analysis shows that a condition for minimum dissipation on the electrode wall is that the field along the insulating segments in the direction perpendicular to the generator axis should be minimized. This requires narrow insulators and (or) fine segmentation. The calculations show that the slant wall does in fact reduce the current near the electrode leading edge, as expected. Strong (rotation) eddy currents are predicted near the apex of the slant wall, which might lead to substantial dissipation in the nonequilibrium plasma. Alternate wall shapes are being sought to minimize these effects.

2.3 Experimental Study of the Interaction of Electrothermal Instabilities with an Insulated Obstacle

An experiment was conducted to simulate the behavior near a segmented-electrode wall, by inserting an insulating obstacle in a square channel with axial current flow and magnetic field normal to its axis. The spaces between the obstacle and the tube walls simulate the electrode surfaces, as current passes through them, while the obstacle itself simulates the insulator segment. A computer simulation of the same geometry was also carried out, with the aim of direct comparison.

The results of the experiment are confusing. Apparently the (unsegmented) cathode and anode at the ends of tube influenced the current pattern more than was expected, so that direct comparison of the experiment and calculation has not so far been possible. Both aspects will be described in detail in the next quarterly report.

2.4 Pulsed Experiment with Molecular Gases

In order to determine the effect of an intense radiation field on the behavior of a nonequilibrium plasma with molecular species, a small, short-time scale experiment has been designed. It consists of a quartz discharge tube, shown in Fig. (4), with end mirrors, a pulsed air core magnet, and apparatus for supplying the tube with He, Cs, CO or CO_2 mixtures. The mode of operation will be as follows: A slow flow of seeded He-CO_2 mixture will be passed through the tube as indicated in the flow schematic of Fig. (5). An axial condenser discharge will produce the plasma on a time scale long compared to that required to produce the ionization and to excite vibrational states, but short compared to that required to heat the gas. A schematic of the electrical system is shown in Fig. (6). Measurements will include axial and Hall fields, Cs continuum radiation, and axial 10.6μ CO_2 radiation. The major components of this apparatus are shown in Fig. (7). Experiments will begin during February or March, 1971.

2.5 Ionization Instabilities in a Magnetohydrodynamic Laser

The two temperature operating regime of the MHD laser will be one in which ionization instabilities would normally be present. These ionization instabilities will be affected by the presence of the lasing radiation field.

In a two temperature plasma with molecular species but without a radiation field which interacts with the molecules, ionization instabilities are not significaily modified by the molecular species. If the excited states of the molecular species are in equilibrium at the gas temperature, the molecular species simply increase the electron heavy particle loss rate without qualitatively changing the nature of the instability. If the molecular species excited states are in equilibrium at the electron temperature, then the effect on the electron gas may be described in terms of a somewhat larger specific heat. The onset condition of the instability should not change for this case but the growth time is lengthened slightly.

When the molecular species interacts with a lasing radiation field, one expects qualitative changes in the behavior of the instability. This is because the electron gas is now coupled through the molecular species to the radiation field and a spatial redistribution of the electron energy is possible. Further, if ionization instabilities persist in the presence of the radiation field, the radiation field will be subject to a 'turbulent' gain distribution within the plasma stemming directly from the nonuniformities resulting from the ionization instability.

The appropriate rate and conservation equation for the CO_2 vibrational system and the electron energy equation including electron excitation of the CO_2 lasing vibrational levels have been formulated along with the Maxwell equations describing the electrical conduction field in the MHD laser and the radiative transport equation describing the radiation field. This description will now be used to study both one and multi-dimensional aspects of the coupling of the two temperature plasma and the lasing radiation field. The effect of the radiation field on the ionization instability will then be examined as well as the effect of the turbulent plasma on the radiation field.

III. DETAILED TECHNICAL CONTRIBUTIONS

3.1 The Three-Dimensional Electrical Conduction Field in a Slanted Electrode Wall MHD Generator

3.1.1. Introduction

In a conventional finitely segmented Faraday connected MHD generator, current concentration effects at electrode edges and over insulators exist which lead to progressively stronger Joule dissipation in these regions as the Hall parameter is increased. These geometrical nonuniformities, induced by the adjacent locations of insulator and conductor segments were first predicted by Hurwitz, Sutton, and Kilb (4), and have been a continual underlying limitation to the electrode wall performance of MHD channels. Although progressively finer segmentation may alleviate the deleterious effects of the conductor insulator nonuniformity in equilibrium gas generators operating with modest Hall parameters, Kerrebrock (5) has shown that these nonuniformities exert a more serious effect on nonequilibrium generators where the excess Joule dissipation at the electrode wall readily elevates the conductivity of the gas near the wall thereby rendering the wall segmentation ineffective.

Ricateau (6) has suggested that the current concentrations in MHD channels with electrode walls parallel to the magnetic field may be alleviated by inclining these electrode walls to the magnetic field. In this way, the current is free to enter the electrode along the magnetic field lines and need not concentrate at the electrode insulator intersections as in the parallel wall case. In the present work we present a detailed study of the electrical conduction field in such a slanted wall channel. In Part 3.1.2 we examine the conditions for minimum Joule dissipation on insulating and conducting surfaces inclined to the magnetic field. In Part 3.1.3 we present the detailed three-dimensional structure of the fields and currents in a slanted wall MHD channel. In Part 3.1.4 we examine the effect of thick velocity boundary layers on the behavior of the current in the slanted wall region. In Part 3.1.5 we show that Hall-effect induced eddy currents resulting from nonuniformities in the magnetic field direction exist even for the case of a uniform gas.

3.1.2 Joule Dissipation on Surfaces Inclined to the Magnetic Field

We consider a gas with conductivity $\overleftrightarrow{\sigma}$ supporting a current $\vec{J}$ with induced field $\vec{E}' = \vec{E} + \vec{U} \times \vec{B}$ where for Cartesian coordinates x, y, z with $\vec{B}$ parallel to the z axis,

$$\vec{J} = \overleftrightarrow{\sigma} \cdot \vec{E}' \tag{1}$$

The conductivity tensor is given by

$$\overleftrightarrow{\sigma} = \begin{bmatrix} \dfrac{\sigma_\perp}{1+\beta^2} & \dfrac{-\beta\sigma_\perp}{1+\beta^2} & 0 \\ \dfrac{\beta\sigma_\perp}{1+\beta^2} & \dfrac{\sigma_\perp}{1+\beta^2} & 0 \\ 0 & 0 & \sigma_\parallel \end{bmatrix} \tag{2}$$

where $\sigma_{\parallel}$ and $\sigma_{\perp}$ are conductivity components and β is the Hall parameter. If we transform from current components (J_x, J_y, J_z) to components (J_x, J_n, J_t) where n and t denote direction normal and tangential to an electrode wall surface inclined to the $\vec{\beta}$ field at angle α, we obtain

$$\begin{bmatrix} J_x \\ J_n \\ J_t \end{bmatrix} = \frac{\sigma_{\perp}}{1+\beta^2} \begin{bmatrix} 1 & -\beta\cos\alpha & -\beta\sin\alpha \\ \beta\cos\alpha & \cos^2\alpha+\frac{\sigma_{\parallel}}{\sigma_{\perp}}(1+\beta^2)\sin^2\alpha & [1-\frac{\sigma_{\parallel}}{\sigma_{\perp}}(1+\beta^2)]\sin\alpha\cos\alpha \\ \beta\sin\alpha & [1-\frac{\sigma_{\parallel}}{\sigma_{\perp}}(1+\beta^2)]\sin\alpha\cos\alpha & \sin^2\alpha+\frac{\sigma_{\parallel}}{\sigma_{\perp}}(1+\beta^2)\cos\alpha \end{bmatrix} \begin{bmatrix} E'_x \\ E'_n \\ E'_t \end{bmatrix} \tag{3}$$

On surfaces where $J_n \equiv 0$ (insulating surfaces), we find from (6) that the normal field and transverse and axial currents are

$$E'_n = -\frac{\beta\cos\alpha}{1+\beta^2\sin^2\alpha} E'_x + \frac{\beta^2\sin\alpha\cos\alpha}{1+\beta^2\sin^2} E'_t$$

$$J_t = \frac{\sigma}{1+\beta^2\sin^2\alpha} (\beta\sin\alpha E'_x + E'_t)$$

$$J_x = \frac{\sigma}{1+\beta^2\sin^2\alpha} (E'_x - \beta\sin E'_t) \tag{4}$$

where we have assumed $\sigma_{\parallel}=\sigma_{\perp}=\sigma$. It is noteworthy that the last two of Eqs. (4) are formally identical to the usual Ohm's Law in the plane perpendicular to $\vec{\beta}$ with β replaced by $\beta\sin\alpha$, i.e., the Hall parameter is based upon the component of $\vec{\beta}$ normal to the plane in which the current vector lies. This formal similarity provides the clue to a requirement for minimum Joule dissipation on insulating surfaces inclined through the magnetic field: given a field E'_x impressed on the surface by the core of the channel, it is necessary that the "Hall field" E'_t be made to vanish. This requirement is clearly seen when the Joule dissipation on the insulating surfaces is considered:

$$\frac{J^2}{\sigma} = \sigma \frac{E'^2_x + E'^2_t}{1+\beta^2\sin^2\alpha} \tag{5}$$

Thus contrary to the usual situation in the core of the channel where maximum recovery of Hall field is desirable, on the inclined insulating wall, it is desirable that the appropriate Hall field E'_t not be recovered at all. The elimination of the Hall field E'_t may be achieved by arranging conducting and insulating segments with fine segmentation relative to the channel width so that the close proximity of conductors imposes a tangential equipotential on adjacent insulating surfaces. We note that if $E'_t=0$, a tangential current will flow on the insulator surface given by

$$J_t = \frac{\beta \sin\alpha}{1+\beta^2 \sin^2\alpha} \sigma E'_x \qquad (6)$$

If the imposition of the tangential equipotential is ineffective and the tangential current J_t is impeded so that $J_t=0$, the tangential field which develops is $E'_t = -\beta \sin\alpha E'_x$. The Joule dissipation in this case is

$$\left(\frac{J^2}{\sigma}\right)_{J_t=0} = 1+\beta^2 \sin^2\alpha \left(\frac{J^2}{\sigma}\right)_{E'_t=0}$$

and for large β is of order of $\beta^2 \sin^2\alpha$ times the dissipation with $E'_t=0$. If the insulating wall is in contact with a core in which full Hall recovery exists and $E_x = (E_x)_{core} = \frac{\beta}{\sigma}(J_y)_{core}$, then the dissipation on the insulator wall relative to the core is

$$\left(\frac{J^2}{\sigma}\right)_{E'_t=0} = \frac{\beta^2}{1+\beta^2 \sin^2\alpha} \left(\frac{J^2}{\sigma}\right)_{core}$$

$$\left(\frac{J^2}{\sigma}\right)_{J_t=0} = \beta^2 \left(\frac{J^2}{\sigma}\right)_{core} \qquad (7)$$

Equations (7) exhibit the crucial features of slanted wall electrodes. For $\beta \gg 1$, the slanted wall ($\alpha \neq 0$) leads to an insulator wall dissipation which is of the order of the core dissipation (provided $E'_t=0$) whereas in the parallel wall case ($\alpha=0$), the insulator wall dissipation is of the order β^2 times the core dissipation. If the condition $E'_t=0$ is not secured and in fact the current J'_t is impeded, the effect of the slanted wall in diminishing the insulator wall dissipation to that of the core will be lost even if $\alpha \neq 0$.

The situation on a conducting surface may be similarly examined. Imposing the equipotential conditions $E_x = 0$, $E_t = 0$ and assuming $E_t = E'_t$ near the wall (the thick boundary layer case), the normal and axial currents are found from Eq. (3) as

$$J_t = \frac{-\beta^2 \sin\alpha\cos\alpha}{1+\beta^2 \sin^2\alpha} J_n$$

$$J_x = \frac{-\beta^2 \cos\alpha}{1+\beta^2 \sin^2\alpha} J_n \qquad (8)$$

The Joule dissipation on the conducting surface is then

$$\frac{J^2}{\sigma} = \frac{1+\beta^2}{1+\beta^2 \sin^2\alpha} \frac{J_n^2}{\sigma}$$

If it is again assumed that the conducting surface is in contact with a core

with full recovery of the Hall voltage and that $J_n \equiv (J_y)_{core}$, we find that

$$\frac{J^2}{\sigma} = \frac{1+\beta^2}{1+\beta^2 \sin^2\alpha} \left(\frac{J^2}{\sigma}\right)_{core} \tag{9}$$

The conducting surface in a slanted wall channel will therefore exhibit dissipation on the order of the core dissipation whereas with $\alpha = 0$, the conductor surface dissipation is of the order β^2 times the core dissipation for $\beta >> 1$.

3.1.3 Detailed Structure of the Electrical Conduction Field

In a finite sized channel the behavior of the current on the conducting and insulating surfaces must be completed by consideration of the nonuniform boundary conditions associated with the location of adjacent insulators and conductors and by the presence of insulating sidewalls in the magnetic field direction. We shall therefore consider the structure of the three-dimensional electrical conduction field subject to the boundary conditions imposed by a finite sized channel with finite segmentation. The Maxwell equations for the small magnetic Reynolds number regime and a time scale for conduction long compared to the plasma frequency period are

$$\nabla_x \vec{E} = 0 \qquad \nabla \cdot \vec{} = 0 \tag{10}$$

We assume the velocity field is such that $\nabla \times \vec{E}' = 0$ and potentials ϕ', ϕ exist such that $\vec{E}' = -\nabla\phi'$, $\vec{E} = -\nabla\phi$. For the case of uniform σ, β Eqs. (1), (3) and (10) reduce to a single elliptic equation for the potential ϕ':

$$\frac{\partial^2\phi'}{\partial x^2} + \frac{\partial^2\phi'}{\partial x^2} + (1+\beta^2)\frac{\partial^2\phi'}{\partial z^2} = 0 \tag{11}$$

We shall apply Eq. (11) to the description of the fields and currents which exist in the chevron shaped slanted wall channel structure of Fig. 1. The boundary conditions applied are those of vanishing normal current on insulating surfaces and specified potentials on conducting surfaces. A single section consisting of one electrode pair of an infinitely long periodic channel may be described by four global variables: the potential difference between the upper and lower electrodes V_y, the potential difference developed in one period in the axial direction V_x, the total current flowing in the electrode pair I_y and the total current flowing in the channel in the axial direction I_x. As shown in Ref. (9), any suitable pair of these global variables V_x, V_y, I_x, I_y determine the complete distribution of field and current within the channel.

On insulating surfaces perpendicular to the magnetic field, the appropriate boundary condition is $\frac{\partial\phi'}{\partial z} = 0$. On the insulating surface within

the slanted electrode wall, the condition for vanishing normal current is

$$\beta\frac{\partial\phi'}{\partial x} + \frac{\partial\phi'}{\partial y} + \tan\alpha\ (1+\beta^2)\frac{\partial\phi'}{\partial z} = 0 \tag{12}$$

The periodicity condition is

$$\phi'(x,y,z) = \phi'(x+\ell,y,z) - V_x \tag{13}$$

The upper conducting surface is at a constant potential $\phi = -V_y/2$. The potentials ϕ', ϕ are related (for uniform magnetic field) by

$$\phi'(x,y,z) - \phi(x,y,z) + B\int_0^y u(\eta)d\eta \tag{14}$$

where $\phi'(x,0,z) = \phi(x,0,z)$. It follows, therefore, that on the conducting surface, the potential ϕ' is given by

$$\phi' = -V_y/2 + B\int_0^{y(z)} u(\eta)d\eta \tag{15}$$

where $y(z)$ is the y coordinate of the slanted wall given by $y(z)=H/2+(a/2-z)\tan\alpha$. The potential distribution for a given velocity distribution may be obtained by substituting the given velocity profile into Eq. (15). We shall consider only two general cases: that of thin boundary layers relative to the channel thickness a and that of thick boundary layers relative to a. For the former we set $u(\eta) = U$ and thus determine

$$\phi' = -V_y/2 + UBH/2 + uB\ (a/2 - z)\tan\alpha \tag{16}$$

For the latter, we set

$$u(\eta) = \begin{cases} U & 0 \leq y \leq H \\ 0 & H < y \end{cases}$$

so that in the thick boundary layer case

$$\phi' = -V_y/2 + UBH/2 \tag{17}$$

In terms of the potential ϕ' the global currents I_x, I_y are

$$I_x = -\int_{-a/2}^{a/2}\int_{-y(z)}^{y(z)} \frac{\sigma}{1+\beta^2}\left(\frac{\partial\phi'}{\partial x} - \beta\frac{\partial\phi'}{\partial y}\right)dy\,dz$$

$$I_y = -\int_{-a/2}^{a/2}\int_{-\ell/2}^{\ell/2} \frac{\sigma}{1+\beta^2}\left(\beta\frac{\partial\phi'}{\partial x} + \frac{\partial\phi'}{\partial y}\right)dx\,dz \qquad (18)$$

and the Joule dissipation is

$$\frac{J^2}{\sigma} = \sigma\left\{\frac{1}{1+\beta^2}\left[\left(\frac{\partial\phi'}{\partial x}\right)^2 + \left(\frac{\partial\phi'}{\partial y}\right)^2\right] + \left(\frac{\partial\phi'}{\partial z}\right)^2\right\} \qquad (19)$$

Since the problem posed is linear for a homogeneous differential equation with partially inhomogeneous boundary conditions, the general solution for any pair of V_x, V_y, I_x, I_y may be obtained by superposition of a fundamental set. This fundamental set of solutions is obtained numerically by iteratively solving a set of finite difference approximations to Eq. (11) and a fundamental set of boundary conditions based upon Eqs. (12), (13), and (16). Details of the numerical technique may be found in Ref. (7).

We shall describe here only results for a Faraday connected channel ($I_x \equiv 0$). For such a channel two performance parameters are of particular interest: the internal impedance R_i and the apparent Hall parameter β_{app}. These are defined as

$$R_i = V_y/I_y$$

$$\beta_{app} = \langle E_x\rangle/\langle E'_y\rangle = (V_x/V_y)(H/\ell)$$

where $\langle\ \rangle$ denotes that each component of the electric field is averaged in its coordinate direction. For a three-dimensional channel, the fields must also be averaged in the magnetic field direction. For a simple arithmetic average, the two expressions for β_{app} corresponding to thick and thin boundary layers are:

$$\text{thin:}\quad \beta_{app} = \frac{V_x}{uB\ell - V_y\frac{\ell}{a}\ln(1+a/H\,\tan\alpha)/\tan\alpha}$$

$$\text{thick:}\quad \beta_{app} = \frac{V_x(a/H)\tan\alpha}{(uBH-V_y)(\ell/H)\ln(1+a/H\,\tan\alpha)}$$

The results to be described are for a modest Hall parameter $\beta=4$ and for a slant wall angle $\alpha=45°$.

Let us consider first the behavior of a slanted wall channel at open circuit. In the thin boundary layer case the induced field $\dot{E}'$ will be shorted by the presence of the conductors. The shorting current appears as a large loop current which leaves the anode near the apex region and enters near the sidewall. For the cathode the pattern is reversed. To study the loop current, the open circuit problem was solved for a fine electrode segmentation ($\ell/H=1/10$). The structure of the open circuit loop current is shown in Fig. 6. The y-z cross section shown intersects the electrode. The current vectors associated with the loop current which lie in the plane of the electrode wall are shown in Fig. 7. The large positive x components of the vectors indicates that the loop is highly three-dimensional. Since the net axial current I_x must be zero, the loop reverses its x direction at some depth within the channel. The distribution of normal current on the electrode wall is shown in Fig. 8. Since this internal circulating loop current remains the same for all loads, it becomes a small fraction of the total generator current at moderate loads if the channel thickness a is small relative to the channel height H.

It is convenient to describe the loaded channel in terms of a load factor $k_y = V_y/UBH$. When the channel is under load, the load current dominates the loop current and the normal current distribution shown in Fig. 9 is obtained. It can be seen that although current concentrations at the electrode edges exist, these concentrations are considerably weaker than those in parallel wall channels at the equivalent segmentation and Hall parameter. It may also be noted that on the edge with the weak singularity, current continues to leave the conductor. This is a result of both the circulating current and the presence of "leakage" [Crown (8), Oliver (9)]. The Joule dissipation shown in Fig. 9 is similarly dimished over that for parallel wall channels except at the apex where strong dissipation exists. This strong dissipation in the apex region is due to Hall effect induced eddy currents which are circulating in the apex region. These eddy currents will be discussed in Part 3.1.5. It can be seen that the potential Φ is quite uniform over the insulator region in the tangential direction running from the apex to the side wall. The field E_t is therefore shorted out and, as discussed in Part 3.1.2, minimum dissipation on the insulator wall is closely achieved. This uniform potential condition results from the rather fine segmentation relative to the channel width which allows the adjacent conductor to impose a tangential equipotential on the insulator. These minimum dissipation effects are reflected in the performance characteristics of this channel:

$$\beta_{app} = 3.24,\ R_i/(R_i)_{ideal} = 1.79$$

where $(R_i)_{ideal}$ is the internal impedance of an infinitely fine segmented channel.

The current vectors on the slanted wall are shown in Fig. 10. It should be noted that the x component of these vectors is small indicating the effectiveness of the slanted wall in inhibiting the axial Hall current. The current patterns in the channel are displayed for several y-z cross sections in Fig. 11. Two trends are present depending on whether the cross section passes through the electrode or through the insulator. For the electrode cross section the current leaves the electrode with a negative z

component. As the current traverses the channel, the current lines curve until the z component is zero. For the insulator cross sections the current initially flows along the insulator with a positive z component. The current lines again curve until the z component is zero. In both instances the curvature occurs within a distance of the order of the electrode width.

A three-dimensional presentation of the current vectors within the channel is shown in Fig. 12. The cross sections are in the x-y plane at four z locations. The sections extend only a depth ℓ into the channel. The variation in the z component of the current vectors evident in Fig. 11 is also present here. An examination of the rows of vectors beneath the "hot edge" shows how sharp the reversal of the z component is.

When these same calculations are carried out for a more coarsely segmented channel (ℓ/a - 1/2), it is found that the internal impedance increases to $R_i/(R_i)_{ideal}$ = 5.22 while the apparent Hall parameter falls to β_{app}=2.04. The potential and current on the electrode wall are shown in Fig. 13 for this case. It can be seen that the Joule heating is more intense and the tangential equipotential on the insulator wall fails consistent with the deterioration in channel performance. The current vector patterns on the slanted wall (Fig. 14) are similar to those for the fine segmentation case; however the vectors for the coarse segmentation case have larger x components associated with them. The current patterns in the y-z cross sections re shown in Fig. 15. The distance over which the current vectors turn to become perpendicular to the magnetic field (z) direction is larger than in the fine segmentation case but still of the order of the electroce width.

3.1.4 Effect of Thick Boundary Layers

If the velocity boundary layers are thick relative to the channel thickness so that the fluid is essentially stagnant in the slanted wall region, then for such a situation, the open circuit loop current will not exist and the shorting effect of $\bar{E}'$ even under load will not be present. Calculations were carried out for the fine segmentation case (ℓ/a=1/10). The values of internal impedance and apparent Hall parameter for the thick layer case were β_{app}=3.20 and $R_i/(R_i)_{ideal}$ = 1.19. Although the apparent Hall parameter is little changed from the thin boundary layer case, the elimination of the internal circulating current improves the internal impedance significantly for the considered geometry in which a = H. The normal current distribution in Fig. 16 exhibits "leakage" indicating that the simultaneous emitter and collector characteristics of the electrode were not due only to the loop current. Analogous to the two-dimensional stagnation point is the line of points with zero current shown in Fig. 7.

3.1.5 The Apex Region

The apex region for the chevron shaped channel is a singular region where a sharp boundary discontinuity in the z direction occurs. Because of the presence of the central symmetry plane z = 0 across which

there is no current flow, the normal and tangential current components diminish to very small values near the apex; however, because of the Hall effect, strong axial current may still flow in the apex region. To improve the resolution near the apex, a finer grid was employed in that region. The results of these refined calculations are shown in Fig. 19. It can be seen that the peaking and diminishment of the normal current as the apex is approached is revealed. The Joule dissipation however exhibits strong singularities on the insulator. These intense regions of Joule heating result from eddy currents which are circulating in the apex region.

The circulation of the current field may be determined from Eqs. (1) and (10) as

$$\nabla_x \vec{J} = -\beta \cdot \nabla \vec{J} + \vec{J} \cdot \nabla \vec{\beta} + (\vec{J} \cdot \nabla \ln\sigma)\vec{\beta} - [\vec{\beta} \cdot \nabla \ln\sigma - \nabla \cdot \beta]\vec{J} \qquad (20)$$

In the case of a general nonuniform gas, the circulation of the current field is proportional to gradients in the conductivity components; however, even for a uniform gas, the presence of boundary induced nonuniformities in the direction of the magnetic field will lead to a rotational current field given by the first term on the right hand side of Eq. (20). We note however that according to Eq. (20) a uniform gas conducting current only in the plane perpendicular to $\vec{\beta}$ will be free of circulation. In Figs. 20 and 21 the current vectors in the plane of symmetry z = 0 are shown. Eddy currents of very high density exist under the insulator. Of particular interest is the circulation component

$$(\nabla_x \vec{J})_z = -\beta \frac{\partial J_z}{\partial z}$$

From Fig. 12 it can be seen that large values of J_z exist close to the plane z = 0 which must fall to zero at z = 0 leading to large values of $\frac{\partial J_z}{\partial z}$ near z = 0. The eddy currents with positive circulation (Fig. 20) may be associated with the negative J_z present in the same region (Fig. 12).

3.1.6 Conclusions

An investigation of the three-dimensional electrical conduction field in a slanted electrode wall MHD generator has shown that a condition for minimum Joule dissipation on the insulator section of the slanted wall is that the tangential electric field E_t' be made to vanish. For a finely segmented channel ($\ell/H = 1/10$) it was shown that a tangential equipotential could be imposed on the insulating section whereas for a coarser segmentation ($\ell/H = 1/2$) the tangential equipotential was not maintained. In the case of thin velocity boundary layers, it was shown that a parasitic internal circulating current exists due to the shorting of the field $\vec{E}'$ by the conductors inclined to the magnetic field. This loop current which dissipates energy within the channel without producing any useful power output degrades the performance of the generator. This performance degradation is evident in the comparison of the internal impedance $R_i/(R_i)_{ideal}$ for thick (1.19) and thin (1.79) boundary layers. The effect of the parasitic current may be diminished by selecting geometries with H >> a.

The original assumption that the slanted electrode wall would relieve the high current densities at the upstream edge of the electrode by allowing the current to enter the electrode along the magnetic field lines is justified by the detailed calculation of the current distribution. In Fig. 21 the current distribution in the slanted wall geometry at the central section of the electrode is compared with results for parallel wall channels. It can be seen that although the slanted wall distributions are for larger Hall parameters $\beta = 4$ they are more uniform than parallel wall distributions at lower Hall parameters $\beta = 2, 3$.

A distinguishing feature of the three-dimensional generator was the existence of circulation within the current field even with uniform conductivity. This circulation was shown to be proportional to the gradients of the current in the magnetic field direction. The eddy currents observed in the apex region where large gradients in J_z exist were an indication of the circulation present. These eddy currents are confined to the apex within a region of the order of the period length ℓ, and hence, for geometries with $\ell/a \gg 1$, the eddy currents may be confined to a locally small region of the wall. For a uniform gas in such geometries they should therefore not seriously affect the overall dissipation on the electrode wall. Indeed, the low values of internal impedance obtained even with the eddy currents present (but with uniform σ, β) are indicative of their minimal effect. In a nonequilibrium gas, however, the high dissipation in the apex region generated by the eddy currents may be sufficient to locally elevate the conductivity and short the plasma rendering the actual segmentation ineffective. Alternate slanted wall arrangements are therefore desirable in which sharp changes of the boundary geometry in the magnetic field direction are avoided while the electrode wall preserves a finite angle relative to the magnetic field.

IV. REFERENCES

1. Research on New Concepts in Energy Conversion, Annual Technical Progress Report No. 1, November 15, 1969.

2. Research on New Concepts in Energy Conversion, Quarterly Technical Progress Report No. 22, March 15, 1970.

3. Kerrebrock, J. L., and Draper, J. S., "Nonequilibrium MHD Generators with Molecular Gases," AIAA Paper No. 70-41, January 19-21, 1970.

4. Hurwitz, H., Sutton, G.,and Tamor, S., "Influence of Tensor Conductivity on Current Distribution in an MHD Generator," J. of Appl. Phys. 32, 2, February 1961.

5. Kerrebrock, J. L., AIAA Journal, Vol. 4, November 1965, p. 1938.

6. Bernard, J., Ricateau, P., and Zettwoog, P., "Effect of Ionization Saturation and Duct Shape on Losses Near Walls," Proceedings of International Symposium on MHD Electrical Power Generator, Salzburg, Austria, July 4-8, 1966.

7. Lowenstein, A. I., "The Performance of a Slanted Electrode MHD Generator," M.S. Thesis, Dept. of Aero. & Astro., Mass. Inst. of Tech., June 1970.

8. Crown, J. C., "Analysis of Magnetohydrodynamic Generators having Segmented Electrodes and Anisotropic Conductivity," United Aircraft Corporation Report R-1852-2, 1961.

9. Oliver, D. A., SUIPR Report No. 163, Institute for Plasma Research, Stanford University, June 1967.

Section II
Figures 1a, 1b: A view of the coaxial-preionizer discharge, taken from the exit of the generator. The lower figure (1a) is a cross-sectional schematic of the preionizer. The top view shows the preionizer in the stratified mode, (with spinning coil), as evidenced by the visibility of the cathode support bar, which is upstream of the discharge, at the sides of the passage. In the second figure, (without spinning coil), the discharge fills the entire channel.

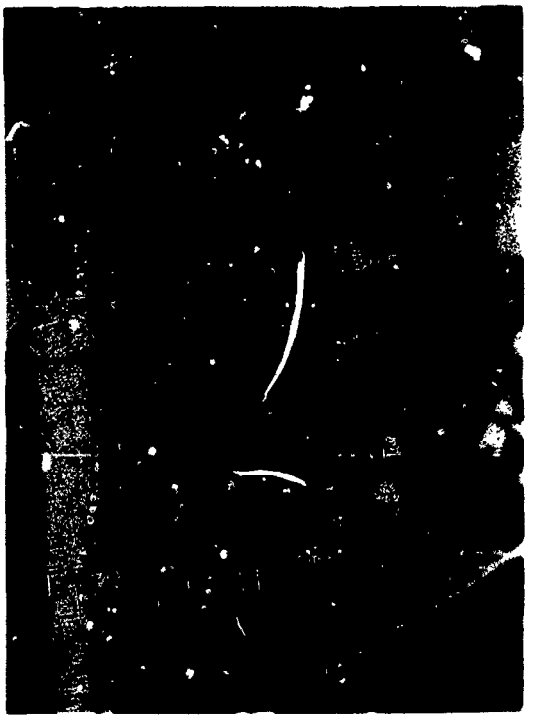

Section II
Figure 2 : Showing the MHD channel, with plexiglass sidewalls, in place in the supersonic wind tunnel.

Section II
Figures 3a, 3b: Shadowgraph pictures of the upstream (3a) and downstream (3b) portions of the channel, showing weak oblique shocks emanating from the nozzle, and comparatively strong normal shocks in the last one fourth of the channel.

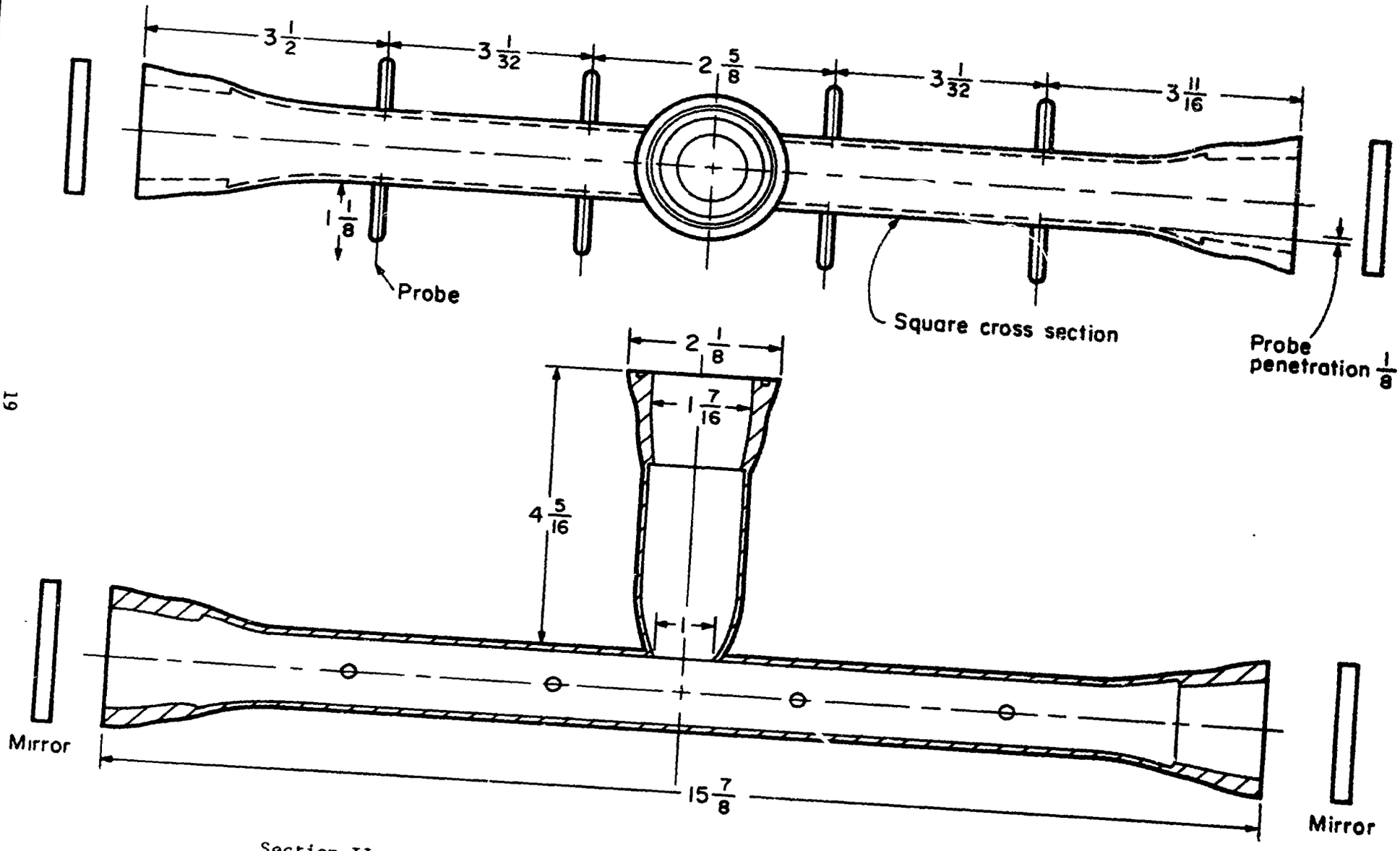

Section II
Figure 4: Discharge tube for pulsed molecular gas experiment, showing locations of probes and mirrors. Dimensions are in inches.

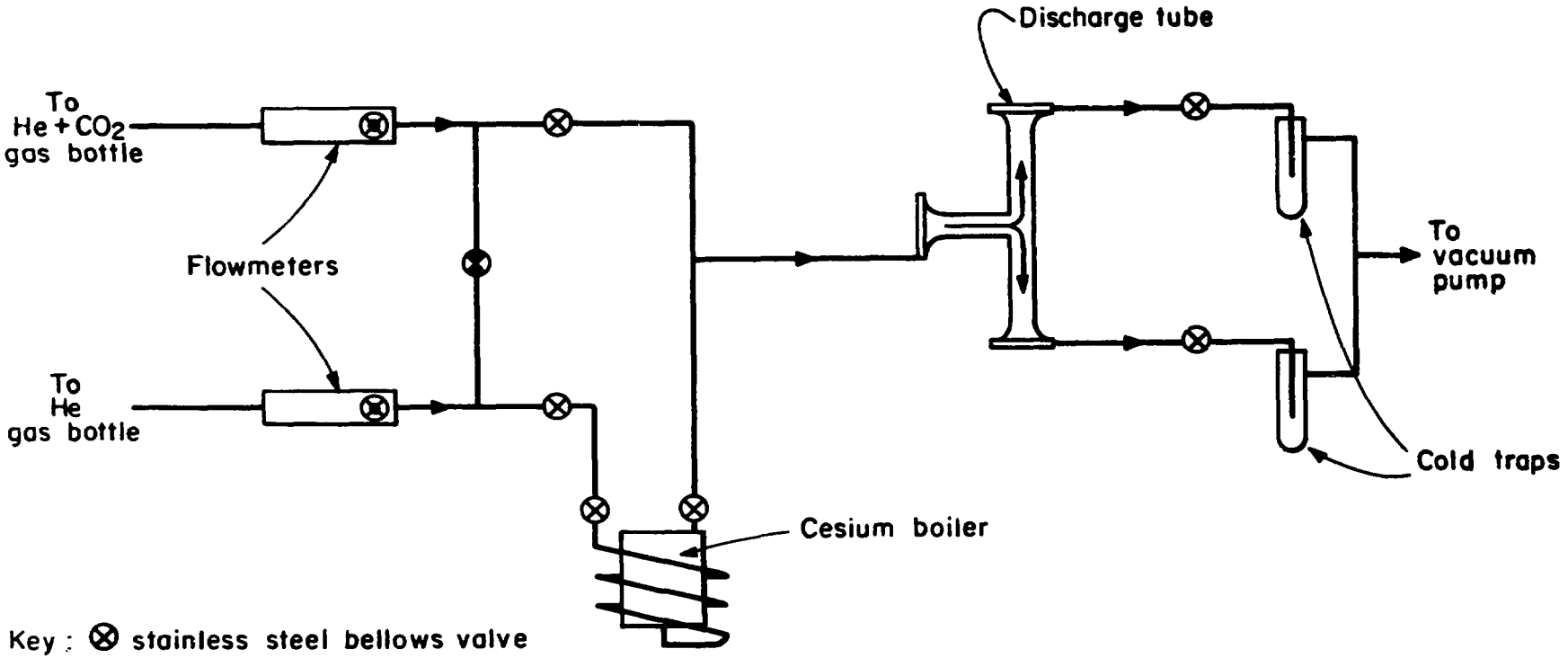

Section II
Figure 5: Flow system for pulsed molecular gas experiment.

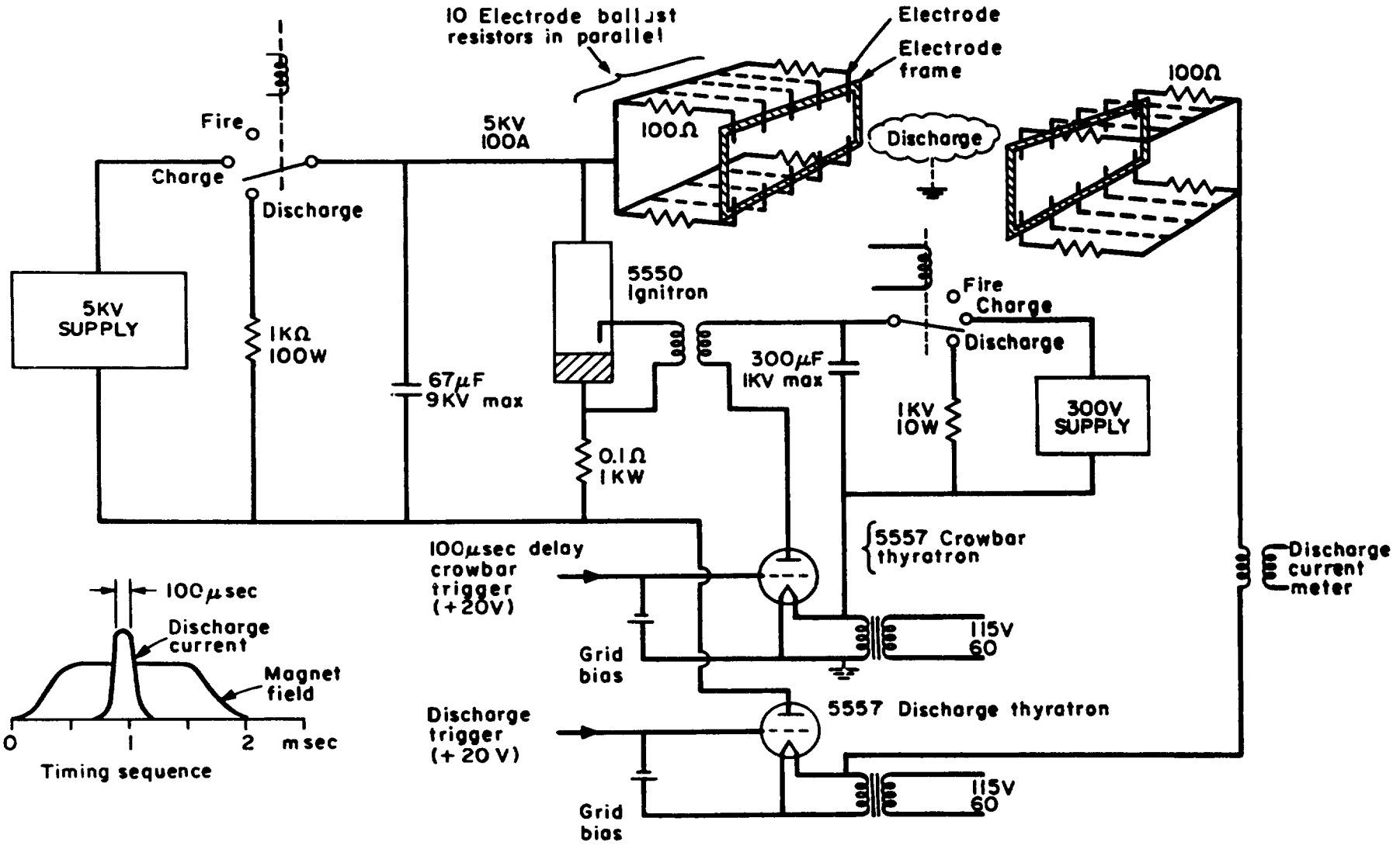

Section II
Figure 6: Electrical discharge system for pulsed molecular gas experiment, including 67μF, 9KV supply, initiating and crowbaring circuits.

Section II
Figure 7: The discharge tube, magnet structure, frame and mirror mounts for the pulsed molecular gas experiment.

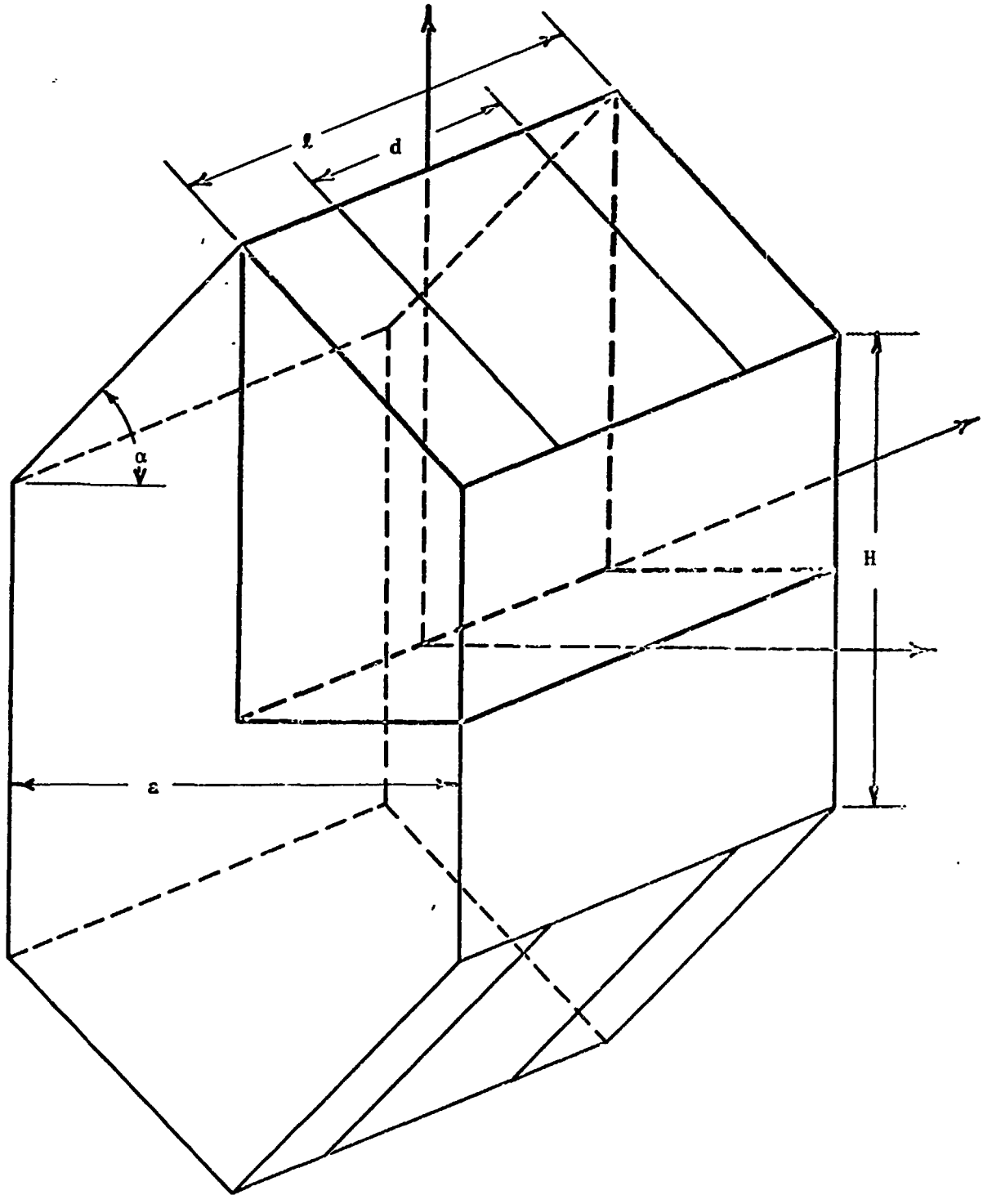

Section III

Figure 1: Schematic of one period length of a slanted electrode MHD channel.

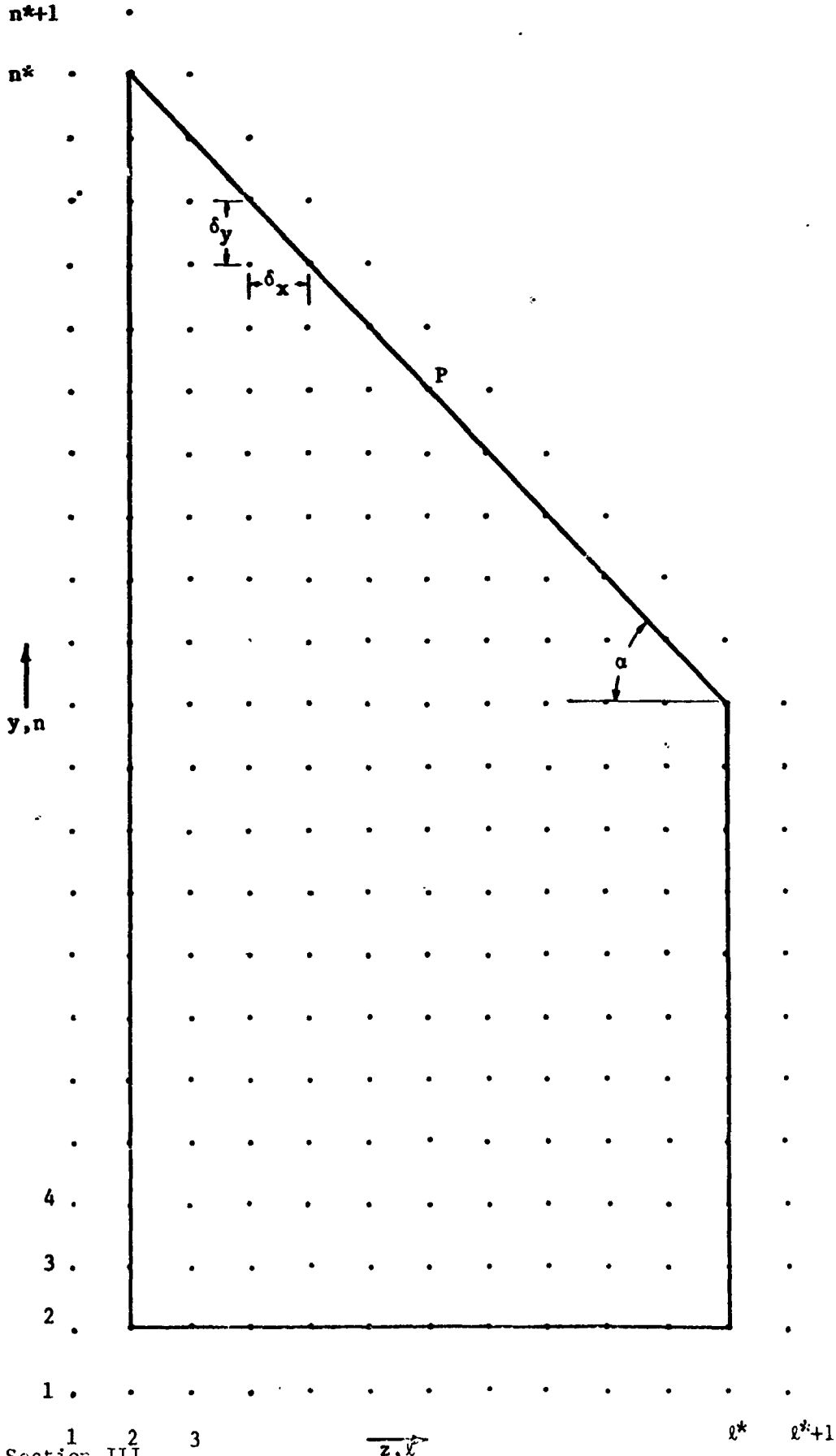

Section III

Fig. 2 Y-Z cross section of channel showing n-ℓ mesh.

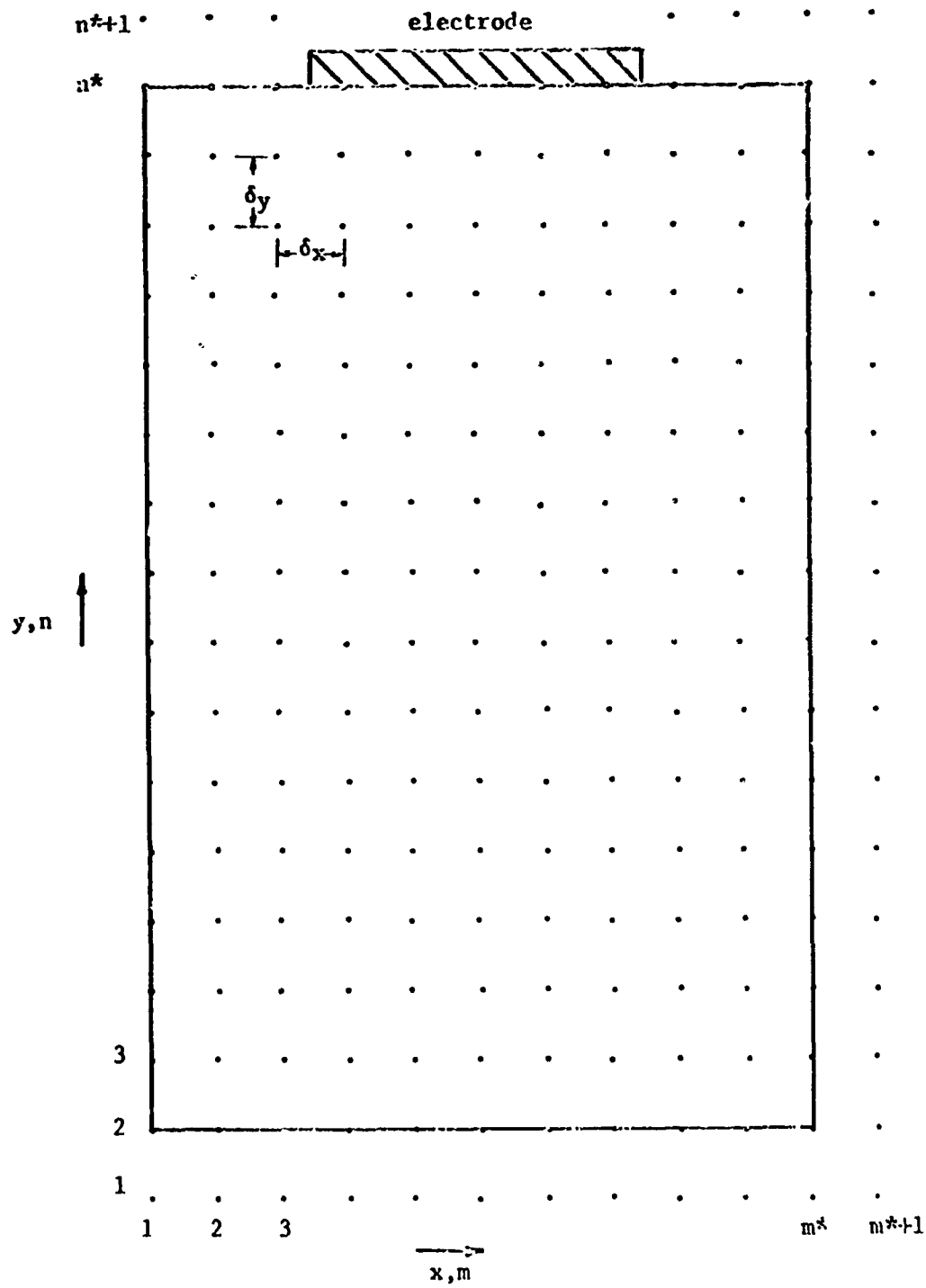

Section III

Figure 3: X-Y cross section of channel showing m-n mesh.

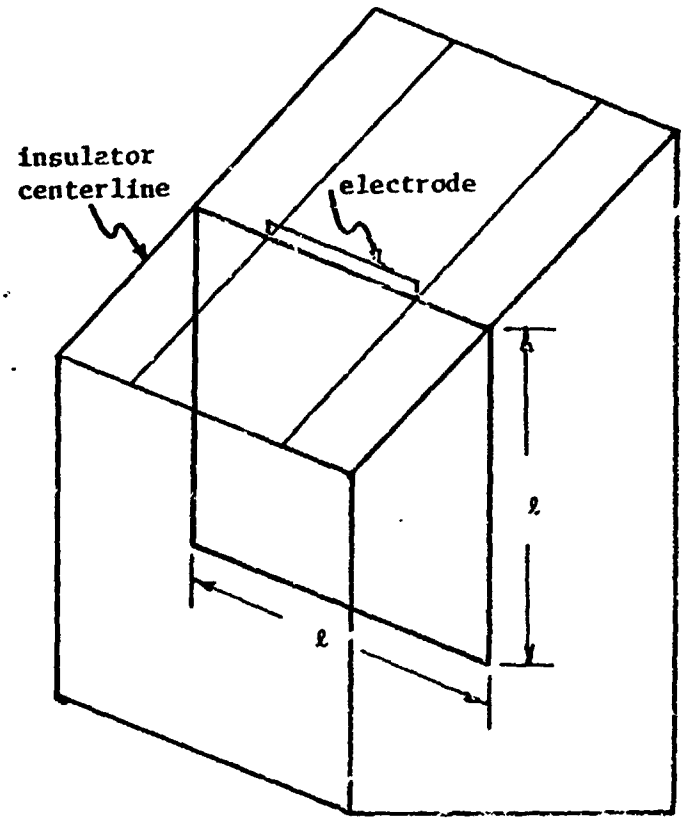

a) Cross section displayed in figure 12.

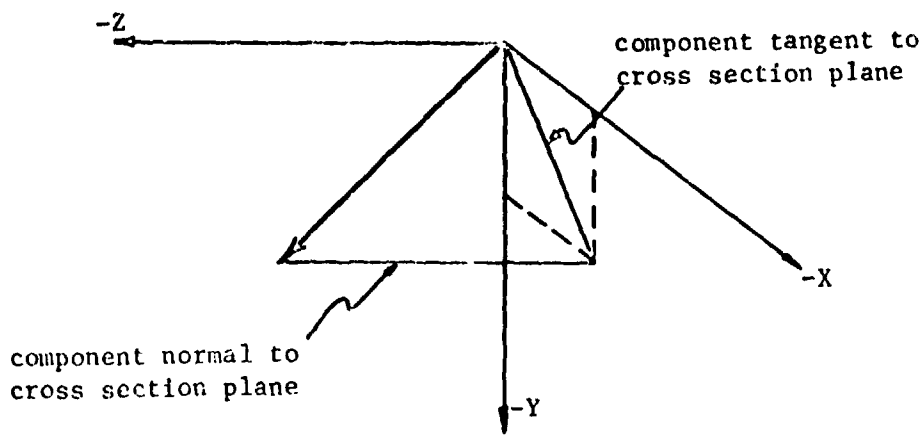

b) Representation of current vector.

Section III

Figure 4: Further explanation for Fig. 12.

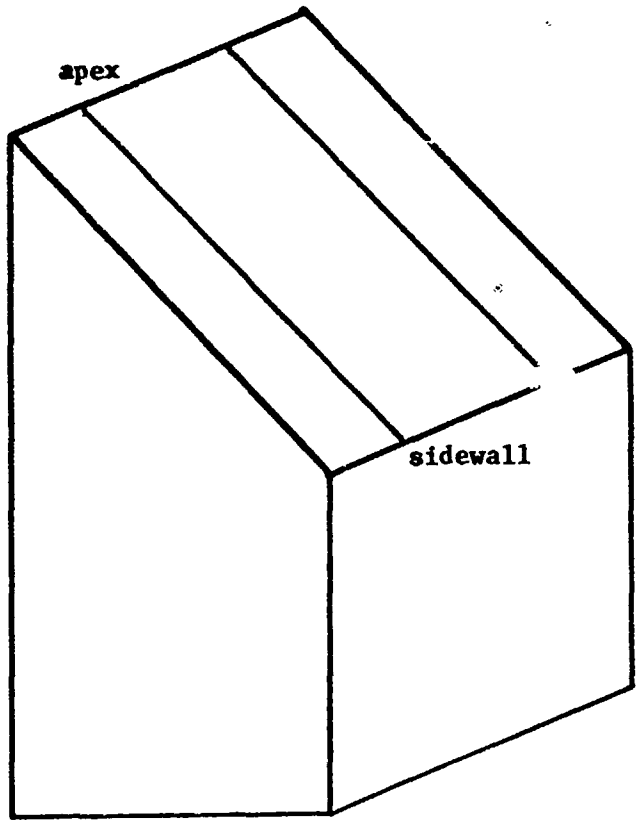

a) Region displayed in slantwall figures.

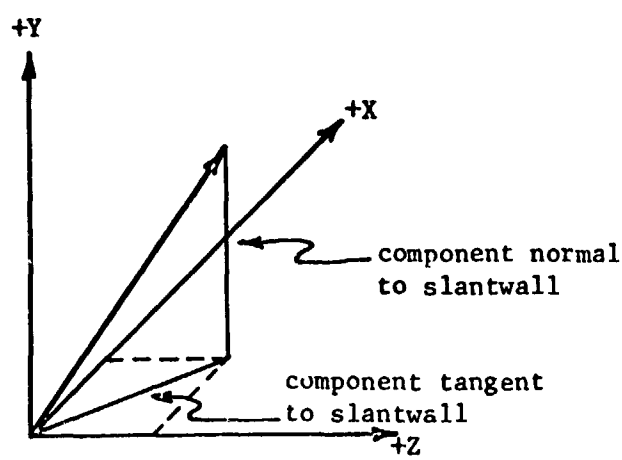

b) Representation of current vector entering electrode.

Section III

Fig. 5 Further explanation for figures displaying current vectors on slantwall.

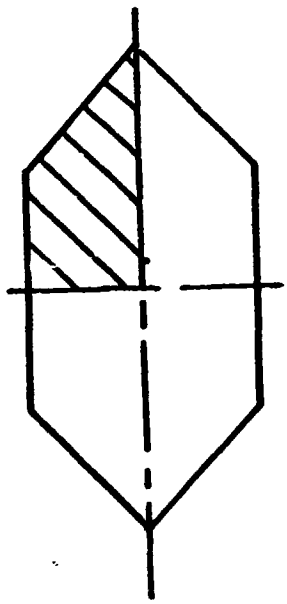

region displayed
in figure

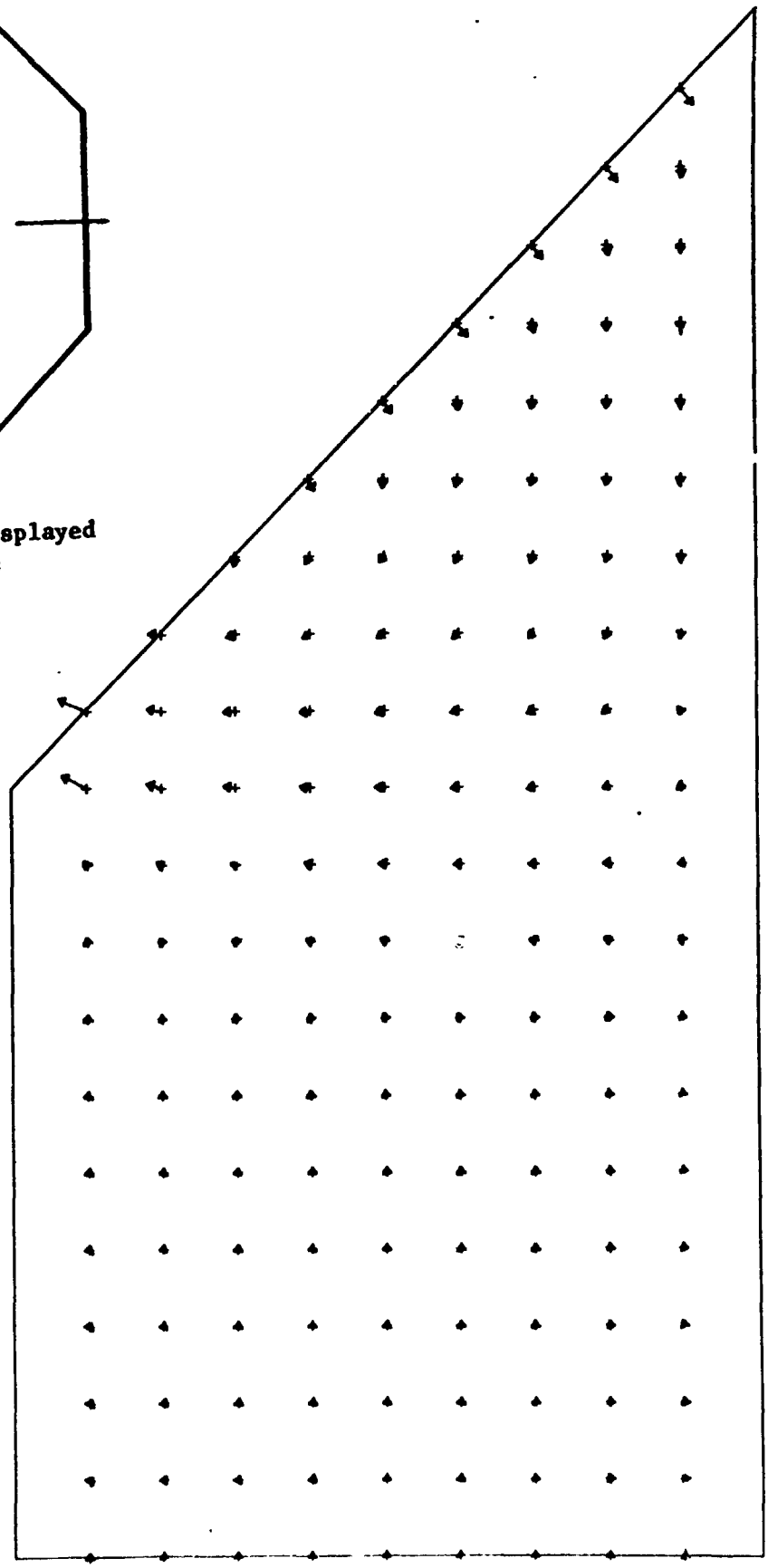

Section III

Fig. 6: Current pattern in y-z cross section. $x/\ell=0.333$
Open circuit, fine electrode segmentation, thin boundary layer.

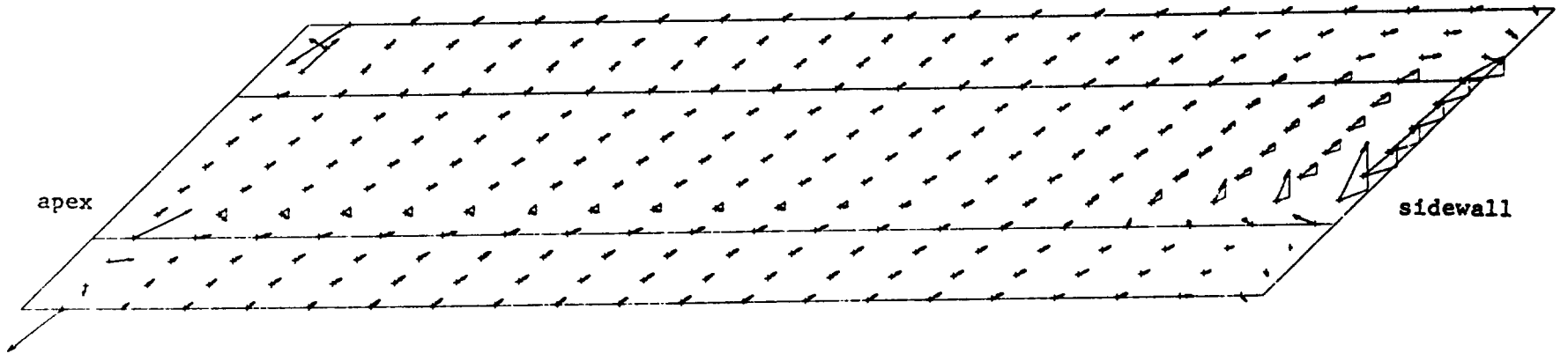

Fig. 7 Current vectors on slantwall.
Open circuit, $\tilde{I}_x = 0$, fine electrode segmentation, thin boundary layer.
(See Fig. 5 for further explanation.)

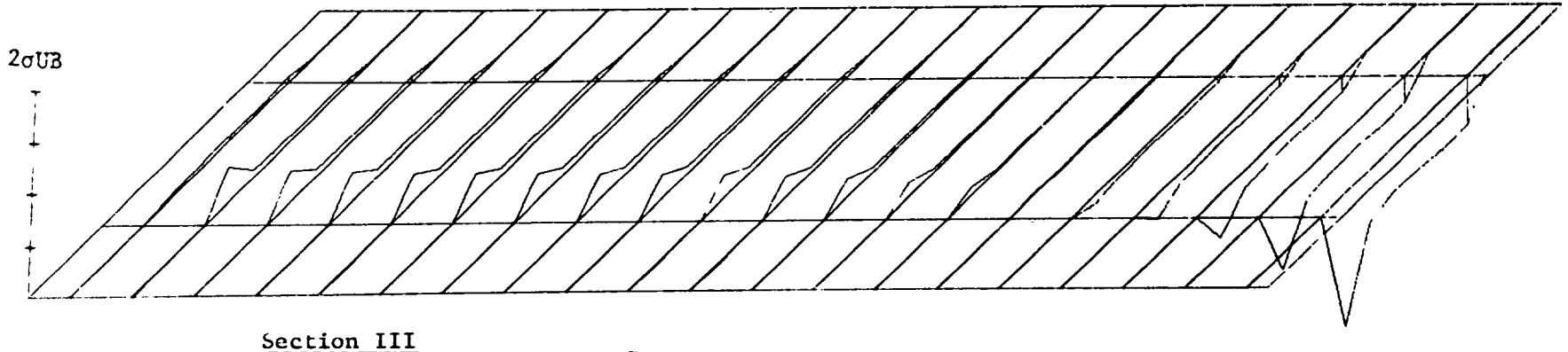

Section III
Figure 8: Distribution of $\tilde{j}_n$ on slantwall.
Open circuit, $\tilde{I}_x = 0$, fine electrode segmentation, thin boundary layer.

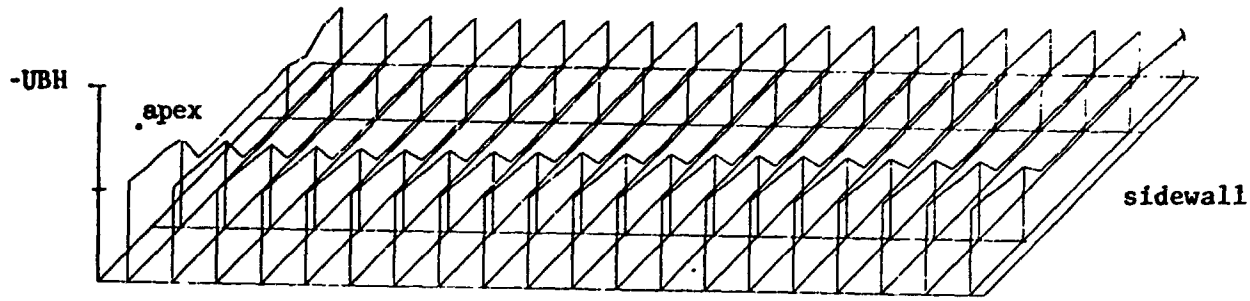

a) phi distribution

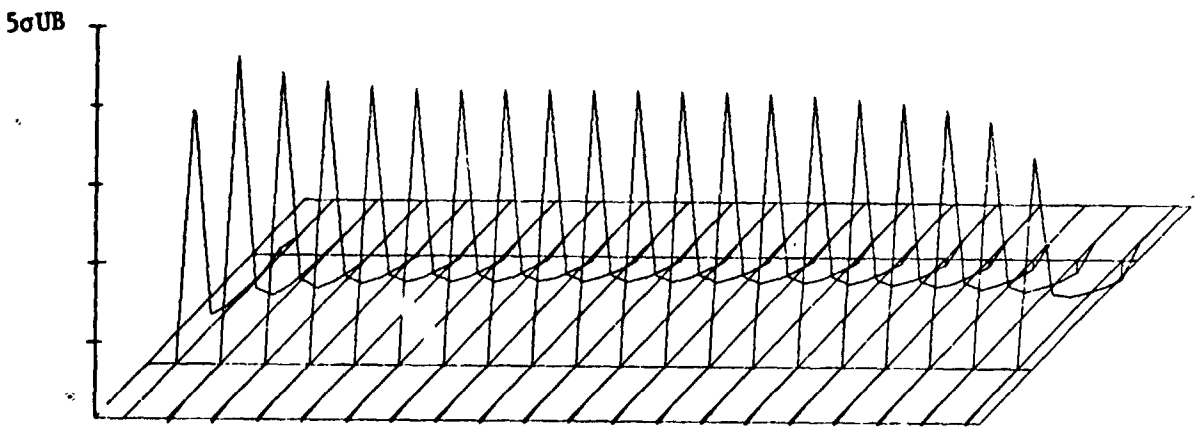

b) $\tilde{j}_n$ distribution

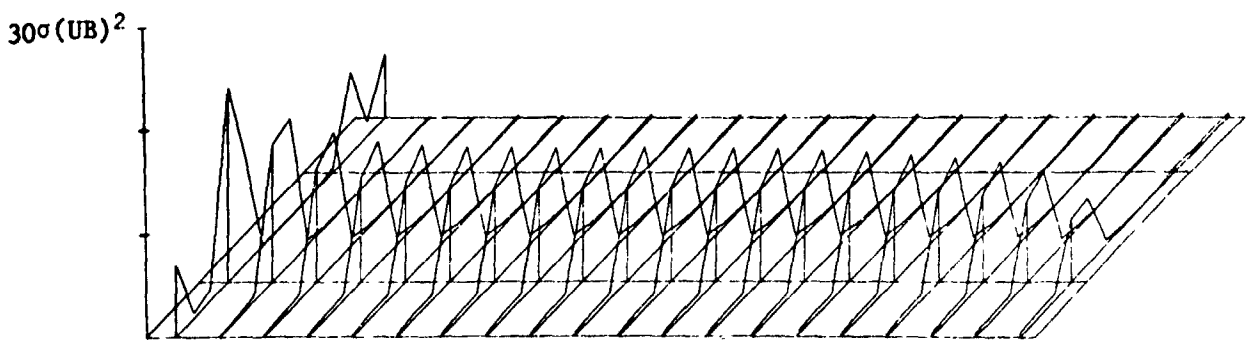

c) Joule dissipation distribution

Section III
Fig. 9: $\tilde{\phi}$, $\tilde{j}_n$, $\tilde{D}$ distributions on slantwall.
$k_y = 1/2$, $\tilde{I}_x = 0$, fine electrode segmentation, thin boundary layer.

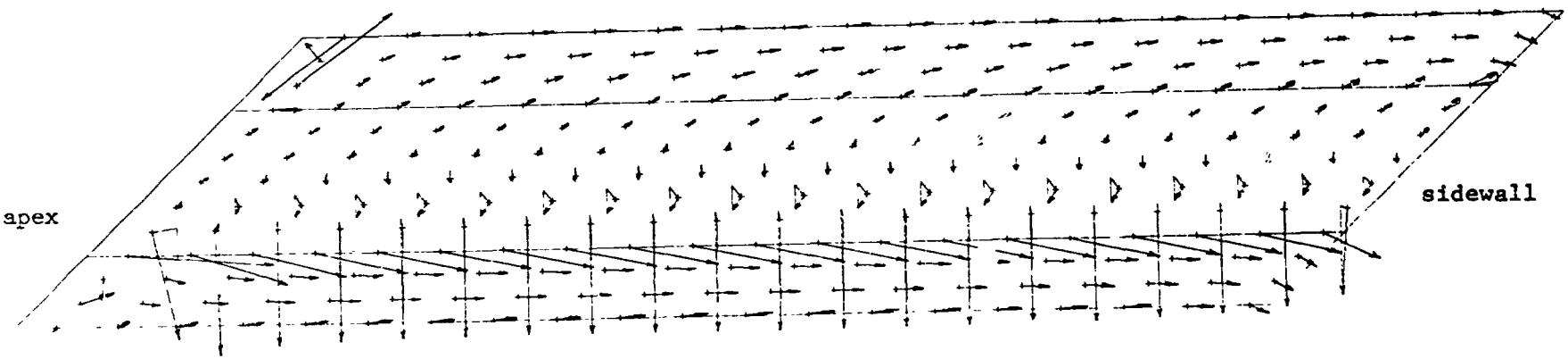

Section III

Fig. 10: Current vectors on slantwall
$k_y = 1/2$, $\bar{I}_x = 0$, fine electrode segmentation, thin boundary layer.
(See Fig. 5 for further explanation.)

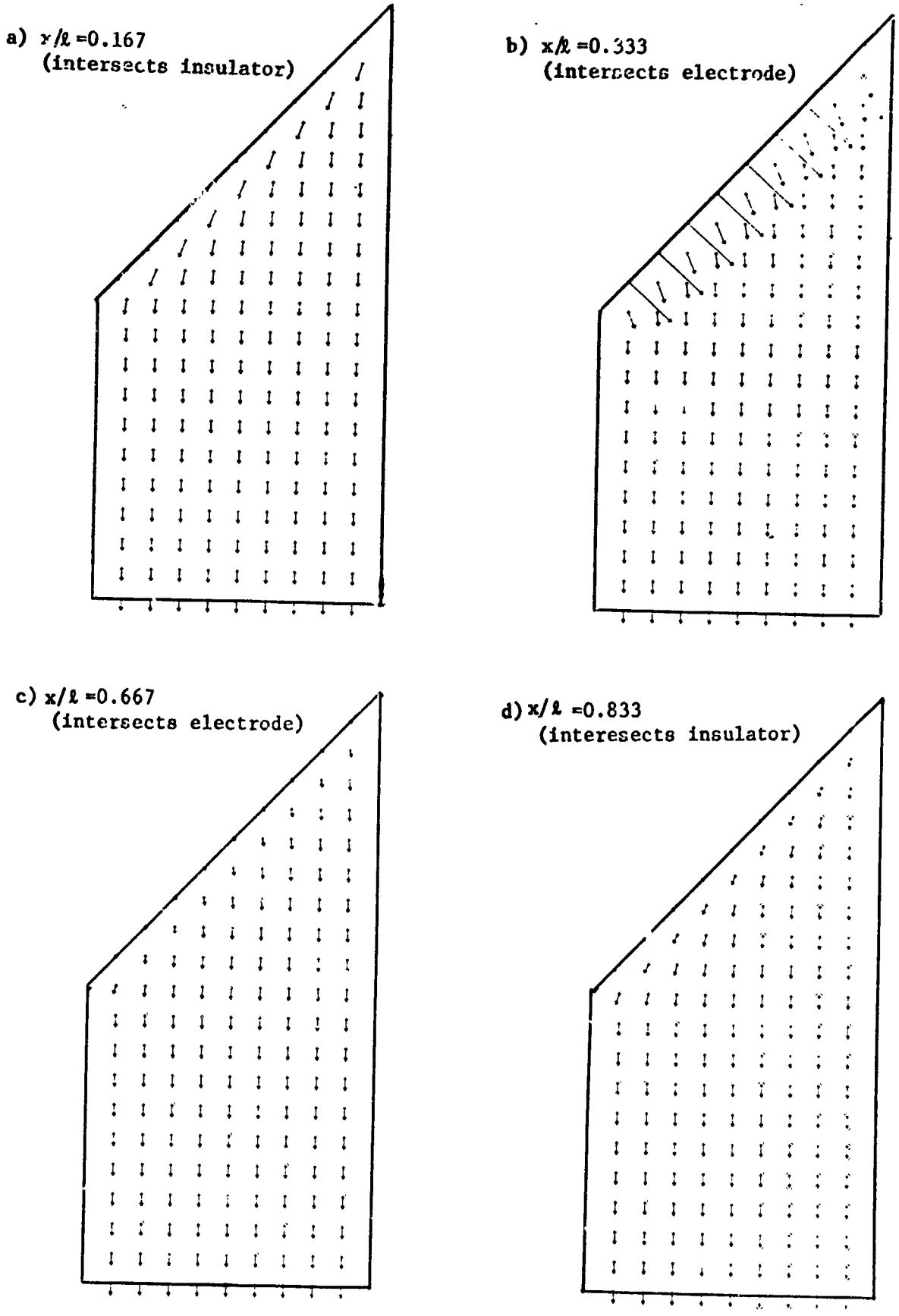

Section III

Fig. 11 Current vector pattern in y-z cross section. k_y=1/2, $\tilde{I}_x$=0, fine electrode segmentation, thin boundary layer.

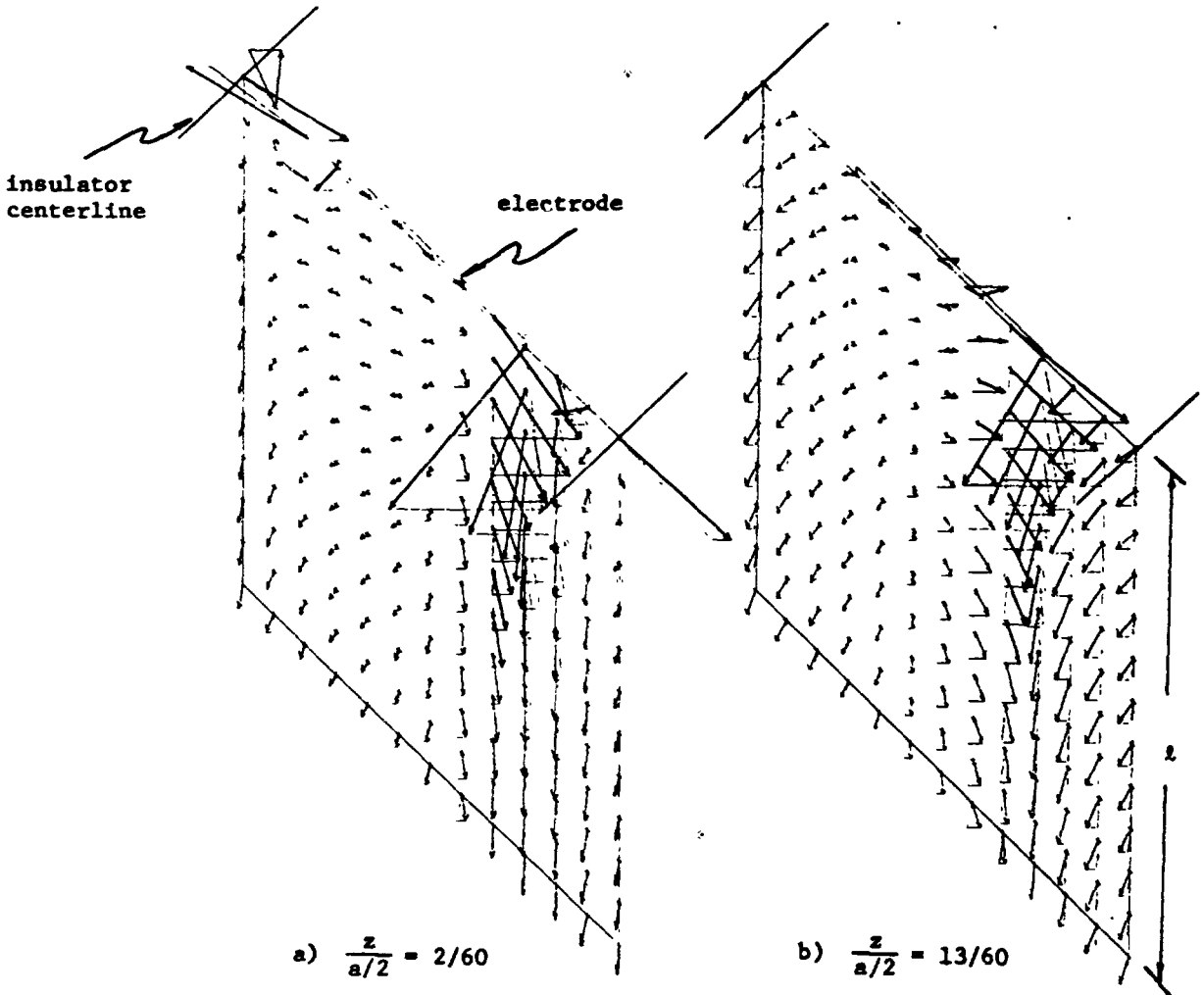

Section III

Fig. 12a,b Current vectors in the x-y plane.
$k_x = 1/2$, $\bar{I} = 0$, fine electrode segmentation, thin boundary layer.
(See Fig. 4 for further explanation.)

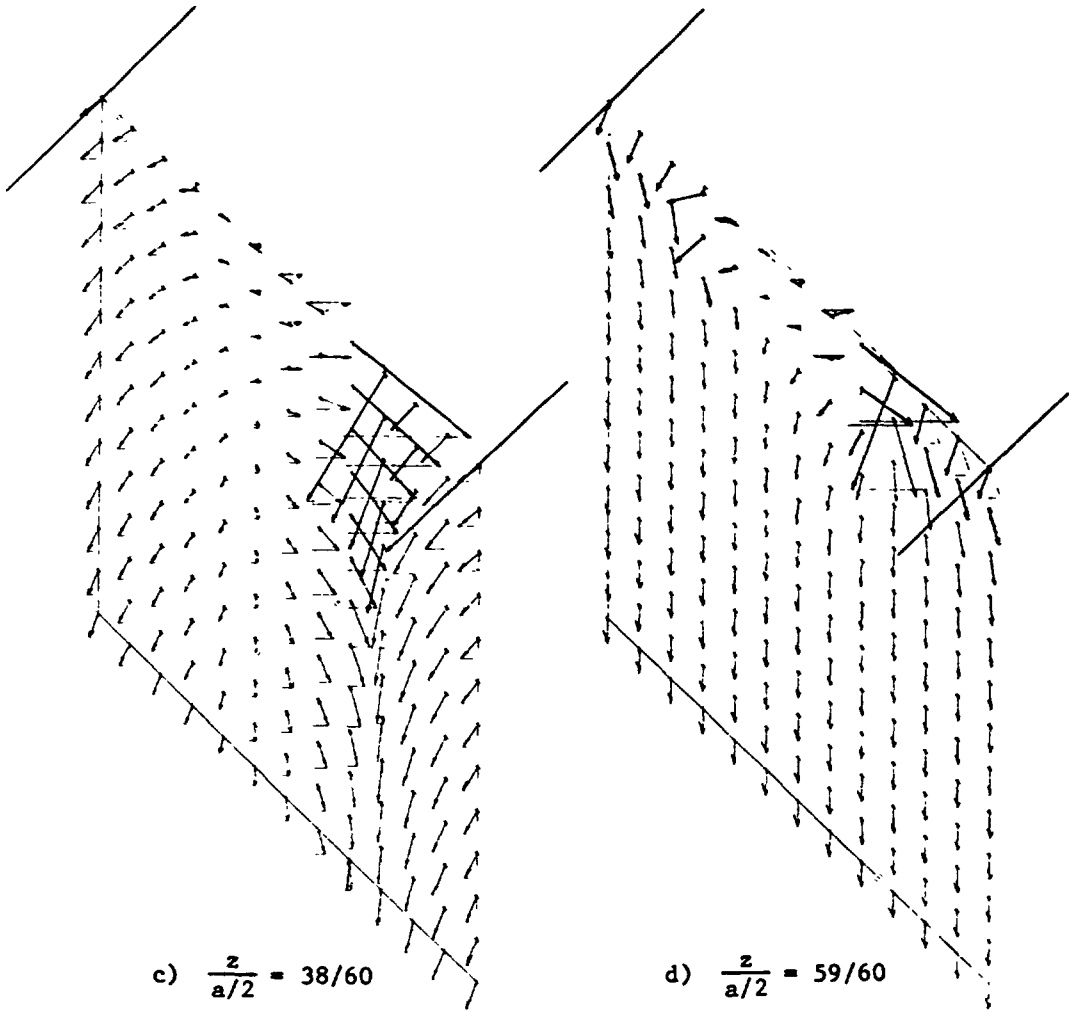

c) $\frac{z}{a/2} = 38/60$ d) $\frac{z}{a/2} = 59/60$

Section III

Fig. 12c,d Current vectors in the x-y plane.
$k_y = 1/2$, $\bar{I}_x = 0$, fine electrode segmentation, thin boundary layer.
(See Fig. 4 for further explanation.)

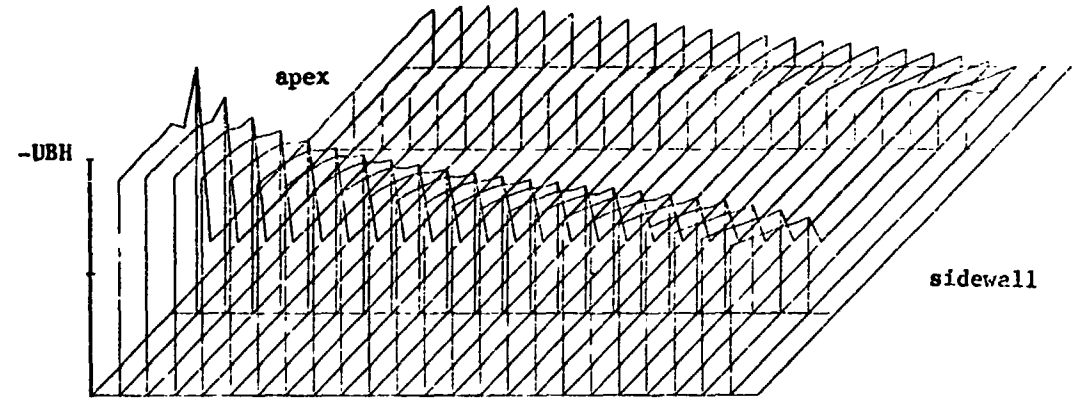

a) phi distribution

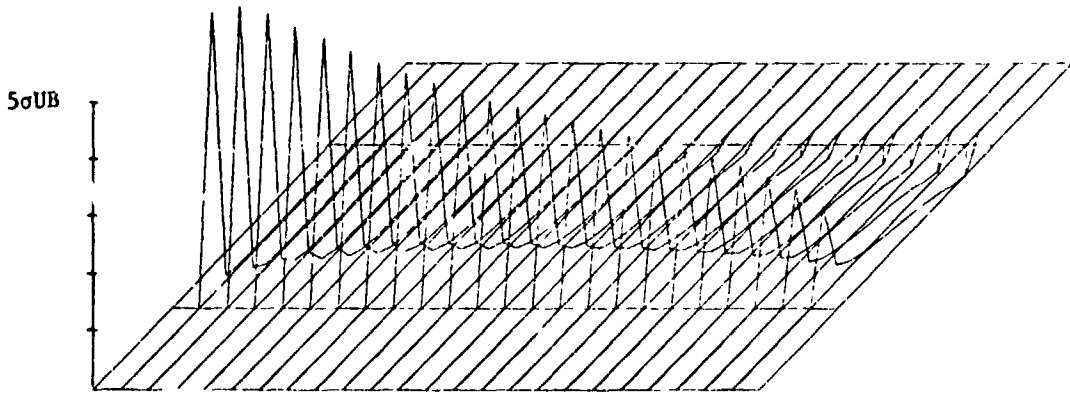

b) $\tilde{j}_n$ distribution

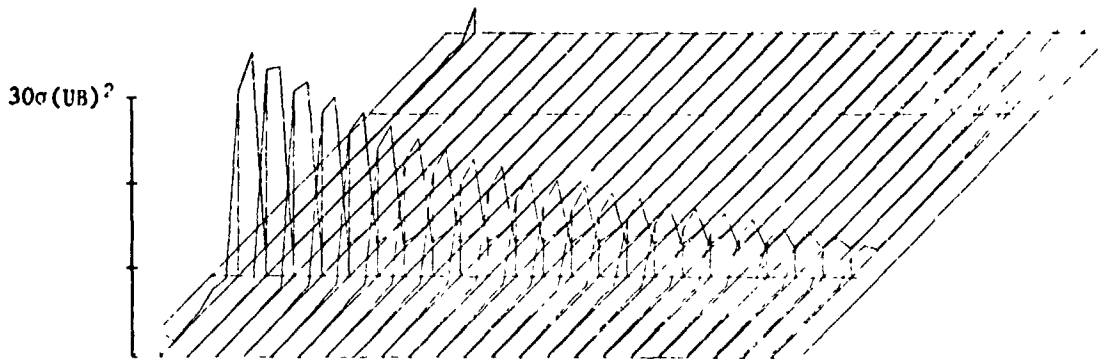

c) Joule dissipation distribution

Section III
Fig. 13 $\tilde{\phi}$, $\tilde{j}_n$, $\tilde{D}$ distributions on slantwall.
$k_y=1/2$, $\tilde{J}_x=0$, coarse electrode segmentation, thin boundary layer.

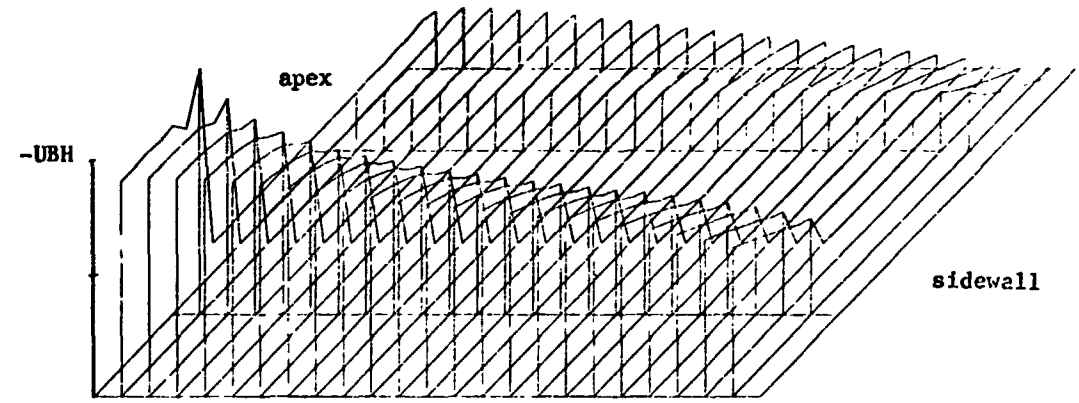

a) phi distribution

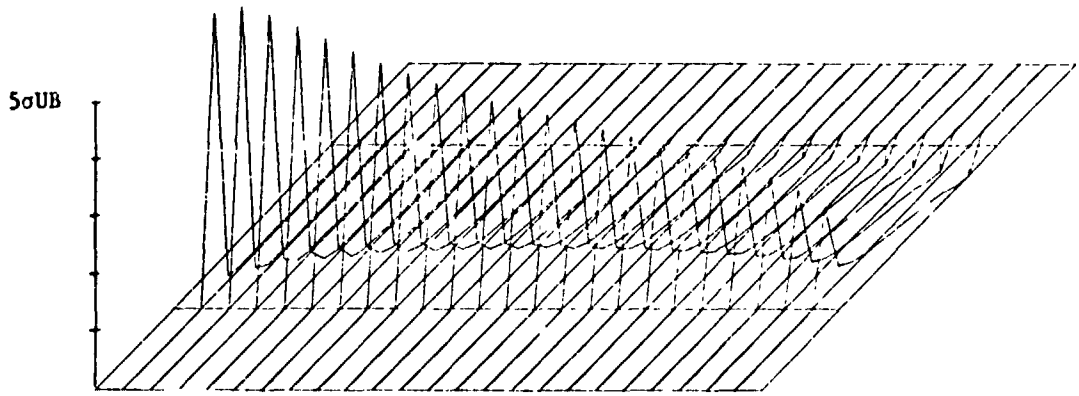

b) $\tilde{j}_n$ distribution

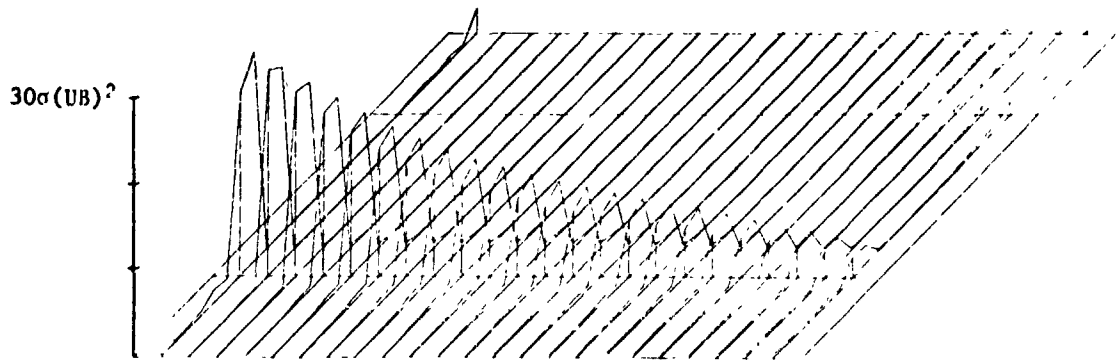

c) Joule dissipation distribution

Section III
Fig. 13 $\tilde{\phi}$, $\tilde{j}_n$, $\tilde{D}$ distributions on slantwall.
$K_y = 1/2$, $\tilde{J}_x = 0$, coarse electrode segmentation, thin boundary layer.

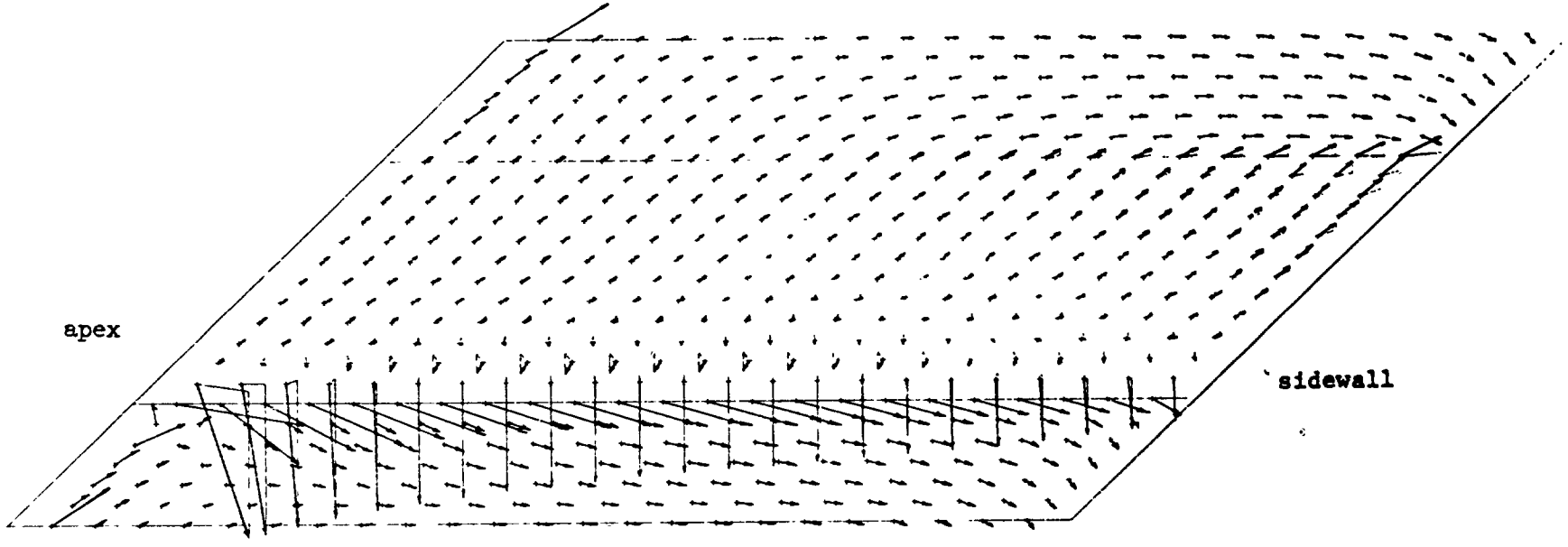

Section III
Fig. 14 Current vectors on slantwall.
k_y=1/2, $\bar{I}_x$=0, coarse electrode segmentation, thin boundary layer.
(See Fig. 5 for further explanation.)

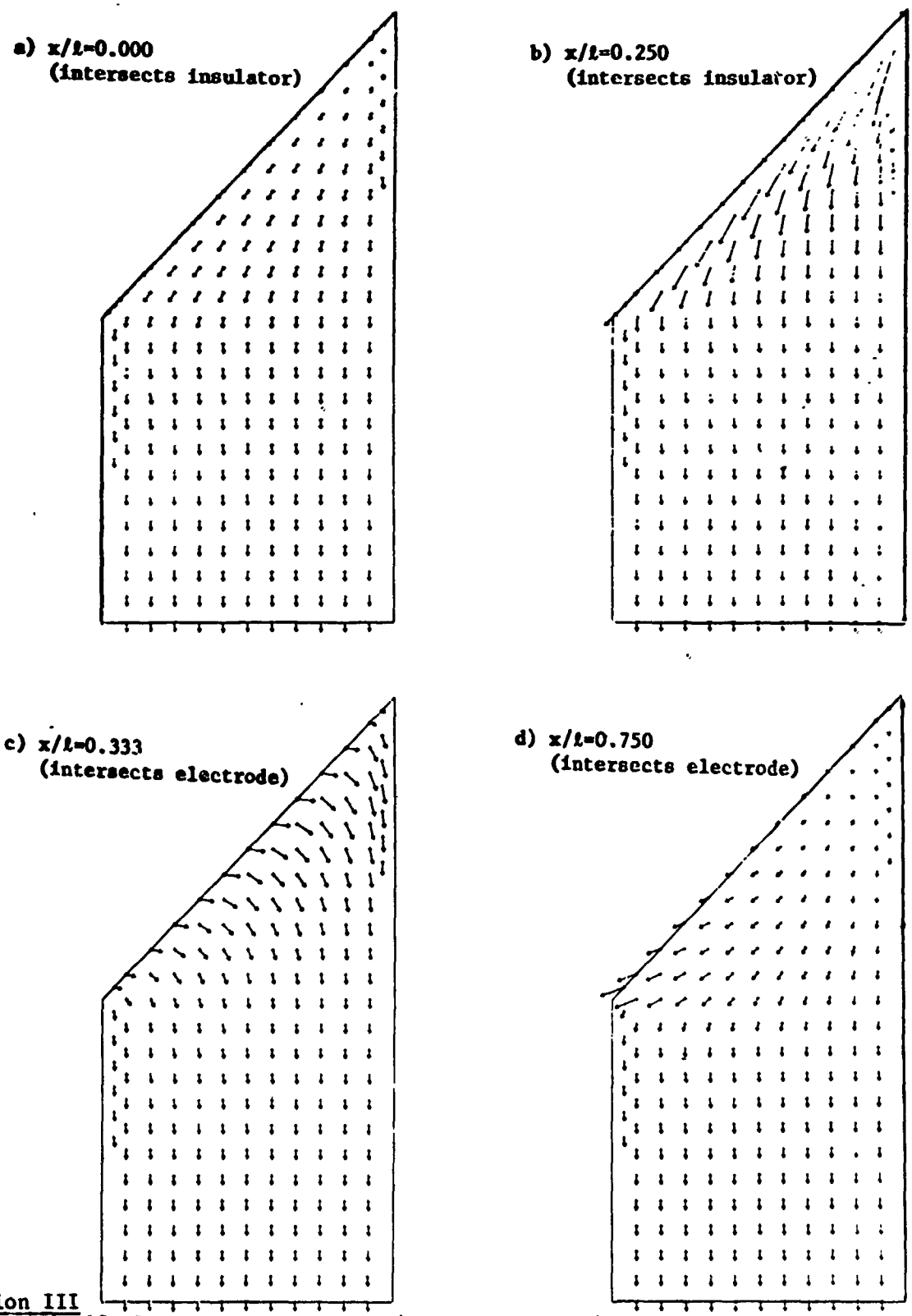

Section III

Fig. 15 Current vector pattern in y-z cross section $k_y=1/2$, $\tilde{I}_x=0$, coarse electrode segmentation, thin boundary layer.

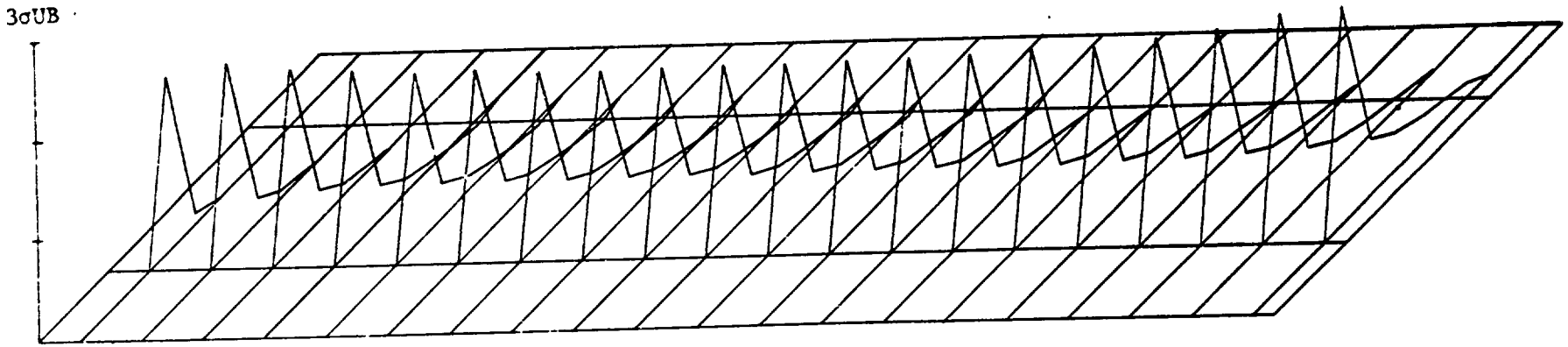

a) $\tilde{j}_n$ distribution

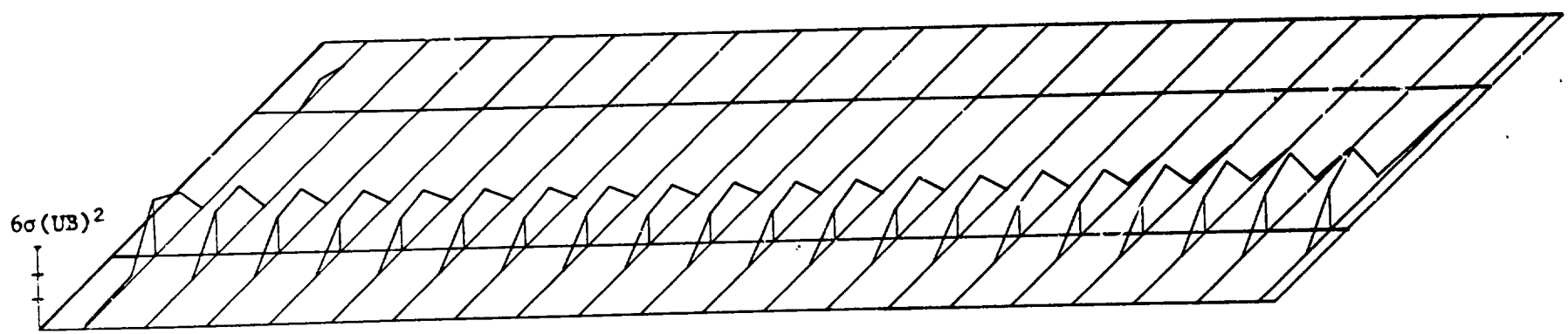

b) Joule dissipation distribution

Section III, Fig. 16 $\tilde{j}_n$, $\tilde{D}$, distributions on slantwall. $k_y = 1/2$, $\tilde{I}_x = 0$, fine electrode segmentation, thick boundary layer.

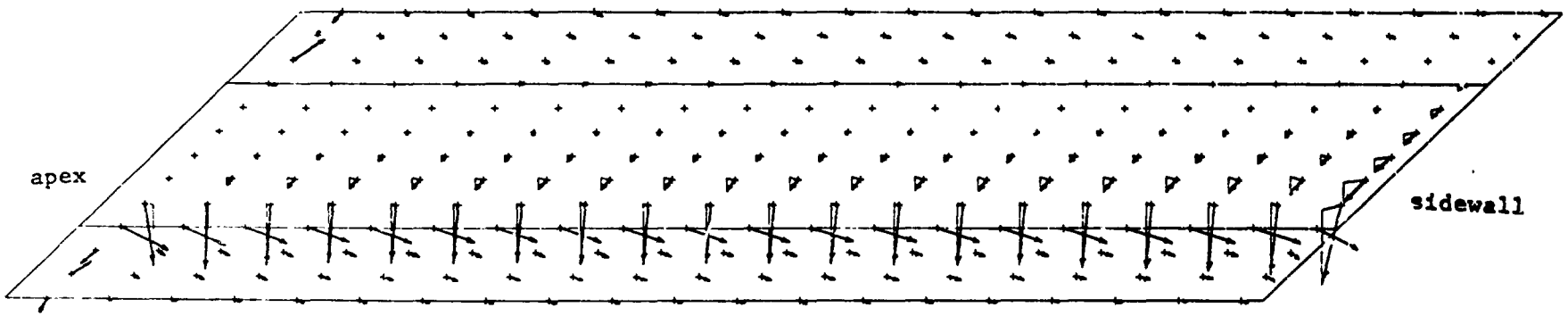

Section III
Fig. 17 Current vectors on slantwall.
$k_y = 1/2$, $\bar{I}_x = 0$, fine electrode segmentation, thick boundary layer.
(See Fig. 5 for further explanation.)

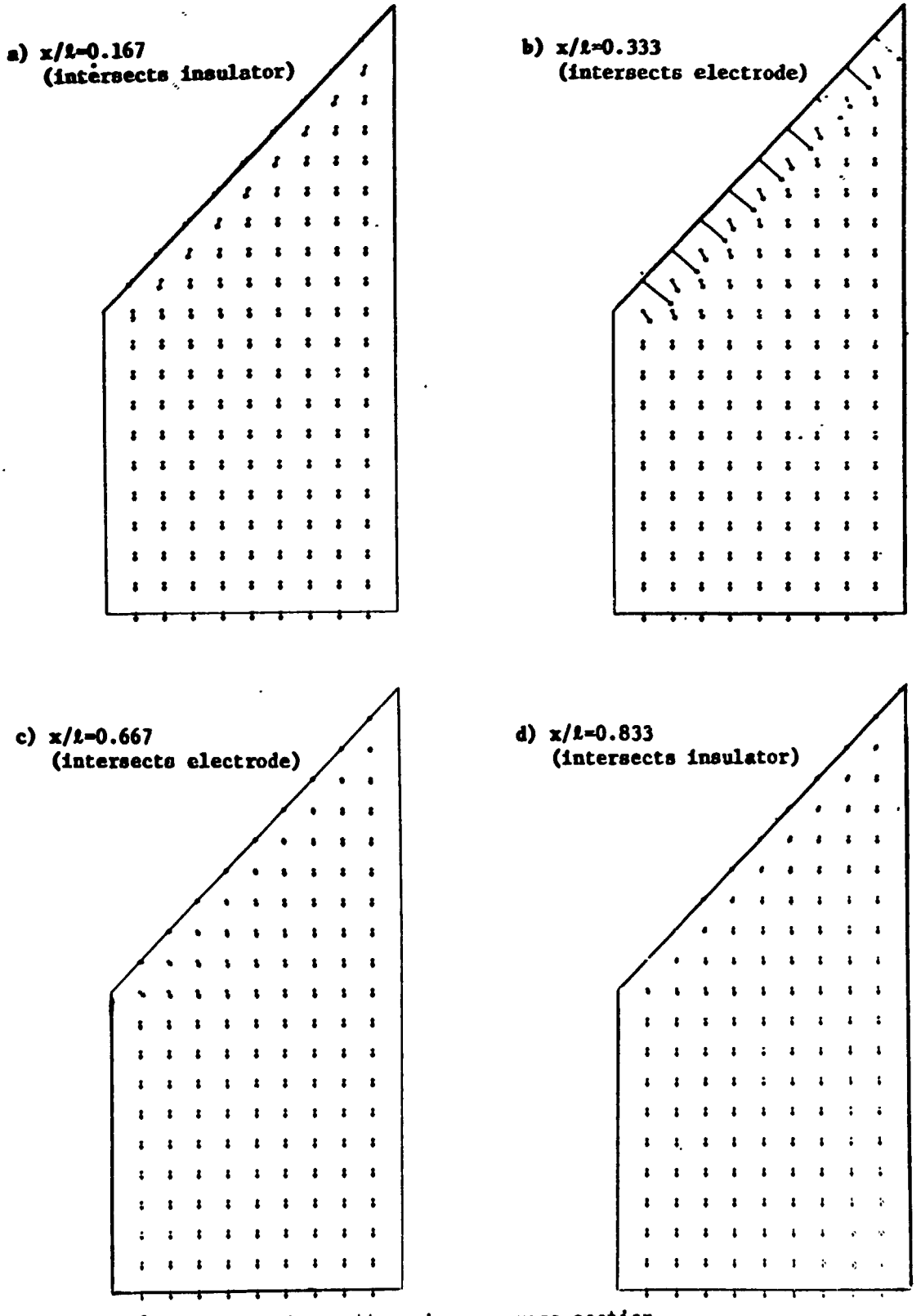

Section III, Fig. 18 Current vector pattern in y-z cross section. $k_y=1/2$, $\bar{I}_x=0$, fine electrode segmentation, thick boundary layer.

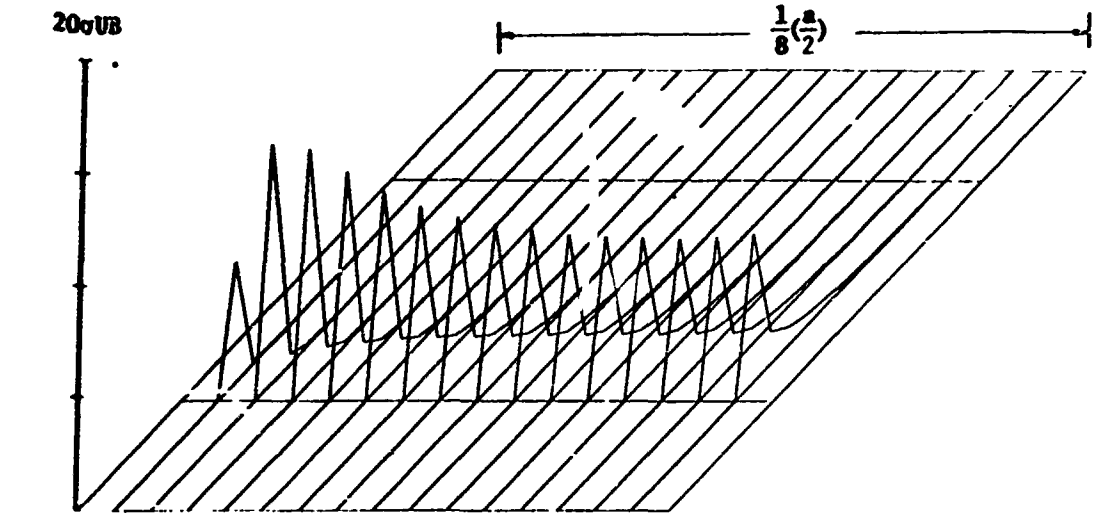

a) $\tilde{j}_n$ distribution

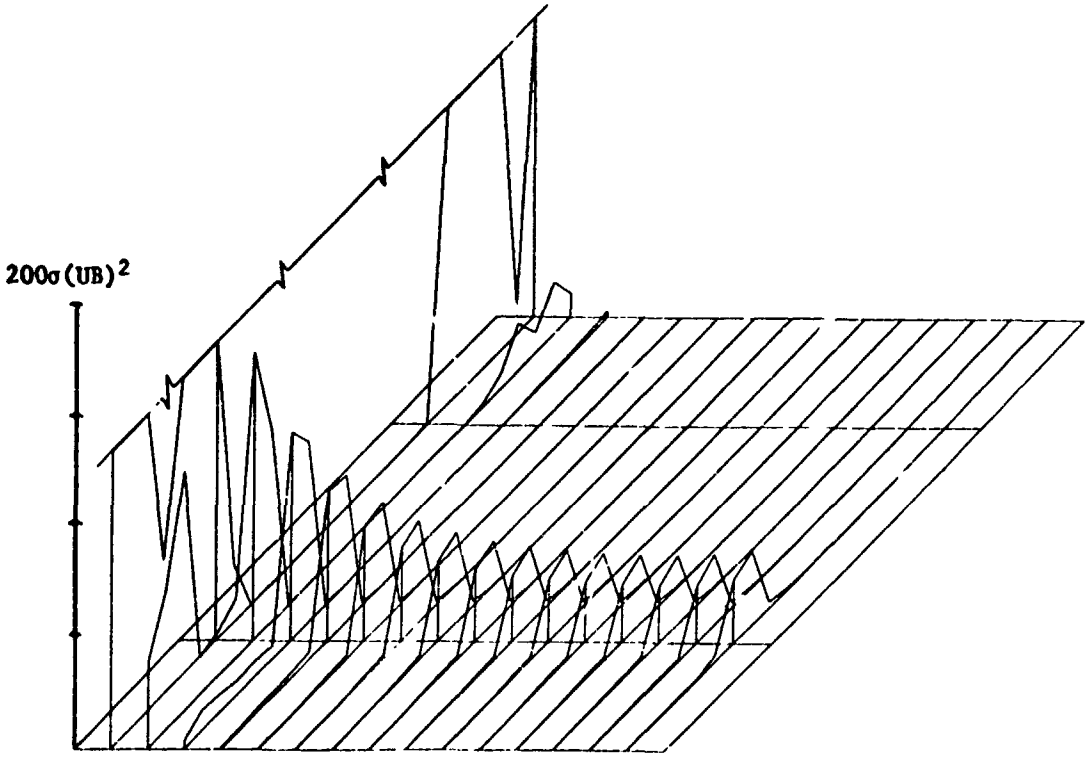

b) Joule dissipation distribution

Section III

Fig. 19 $\tilde{J}_n$, $\tilde{D}$ distributions on slantwall. Apex analysis. $k_y=1/2$, $\tilde{I}_x=0$, fine electrode segmentation, thin boundary layer.

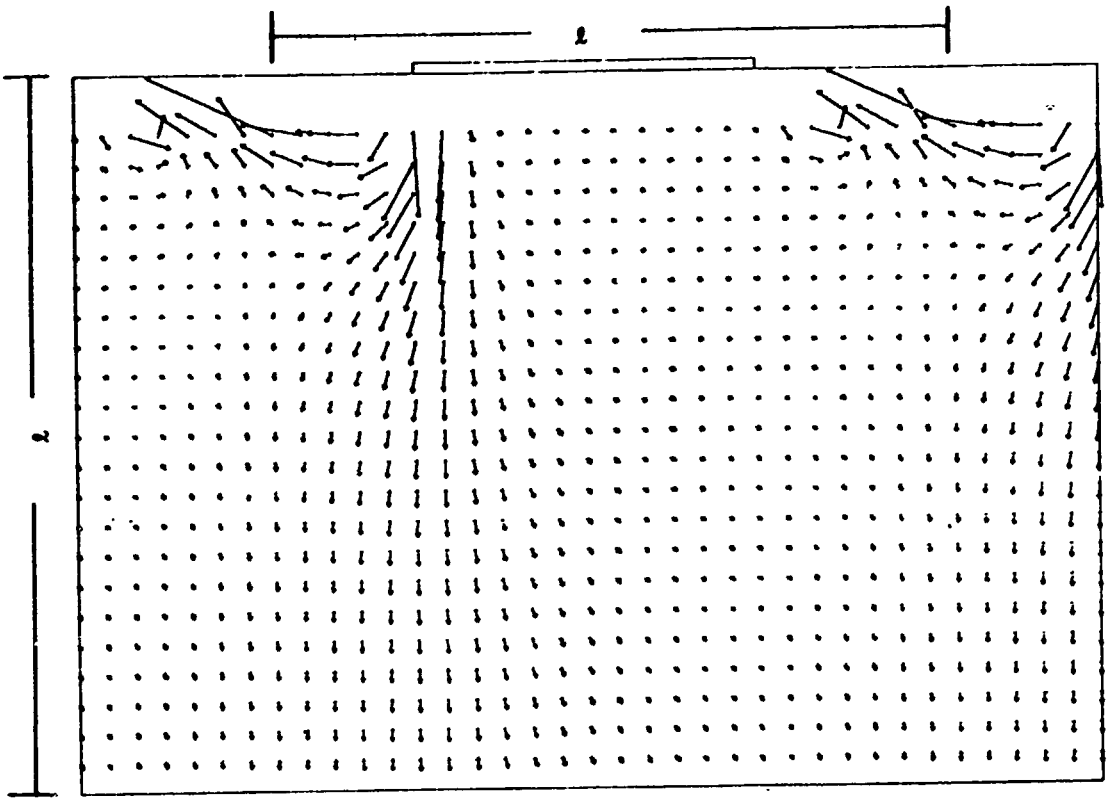

a) thin boundary layer

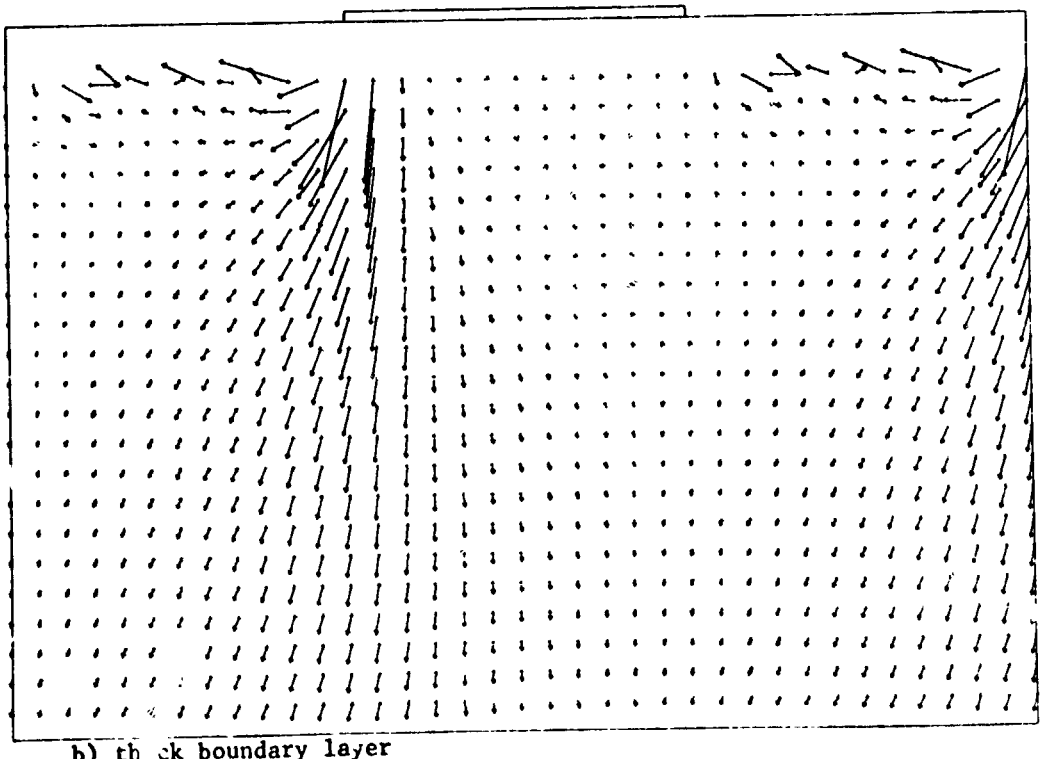

b) thick boundary layer

Section III
Fig. 20 Current pattern in symmetry plane.
k = 1/2, $\tilde{I}_x = 0$, fine electrode segmentation.

Three dimensional channel $\beta = 4$

1. thin boundary layer, fine segmentation, $k_y = 1/2$, $\tilde{I}_x = 0$
2. thick boundary layer, fine segmentation, $k_y = 1/2$, $\tilde{I}_x = 0$
3. thin boundary layer, coarse segmentation, $k_y = 1/2$, $\tilde{I}_x = 0$

Two dimensional channel

4. Oliver (Ref. 3) $\beta = 3$
5. Celinski and Fisher (Ref. 2) $\beta = 2$

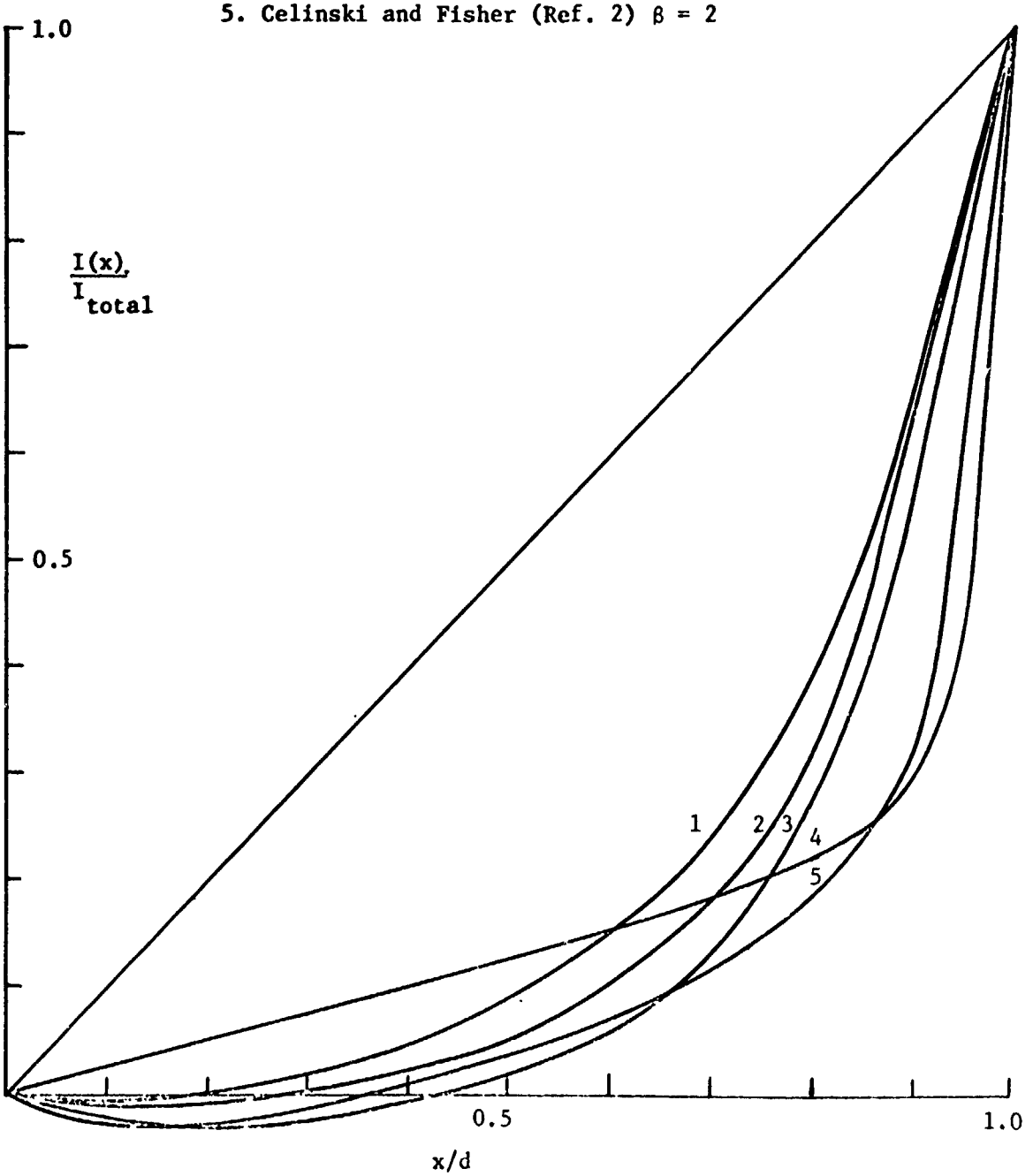

Section III
Fig. 21 Current distribution on Electrode. $\frac{I(x)}{I_{total}}$ vs. $\frac{x}{d}$